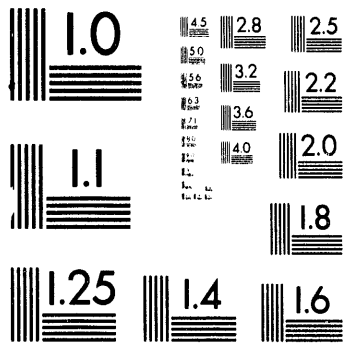
1.0
1.1
1.25
1.4
1.6
1.8
2.0
2.2
2.5
2.8
3.2
3.6
4.0
4.5
5.0
5.6
6.3
7.1
8.0
9.0

1 of 1

Conf-9309228--7

UCRL-JC-114791
PREPRINT

The Impact of Repository Heat on Thermo-Hydrological Performance at Yucca Mountain

Thomas A. Buscheck
John J. Nitao

This paper was prepared for submittal to
the American Nuclear Society
Topical Meeting on
Site Characterization and Model Validation
(FOCUS '93)
September 26–29, 1993
Las Vegas, Nevada

September 1993

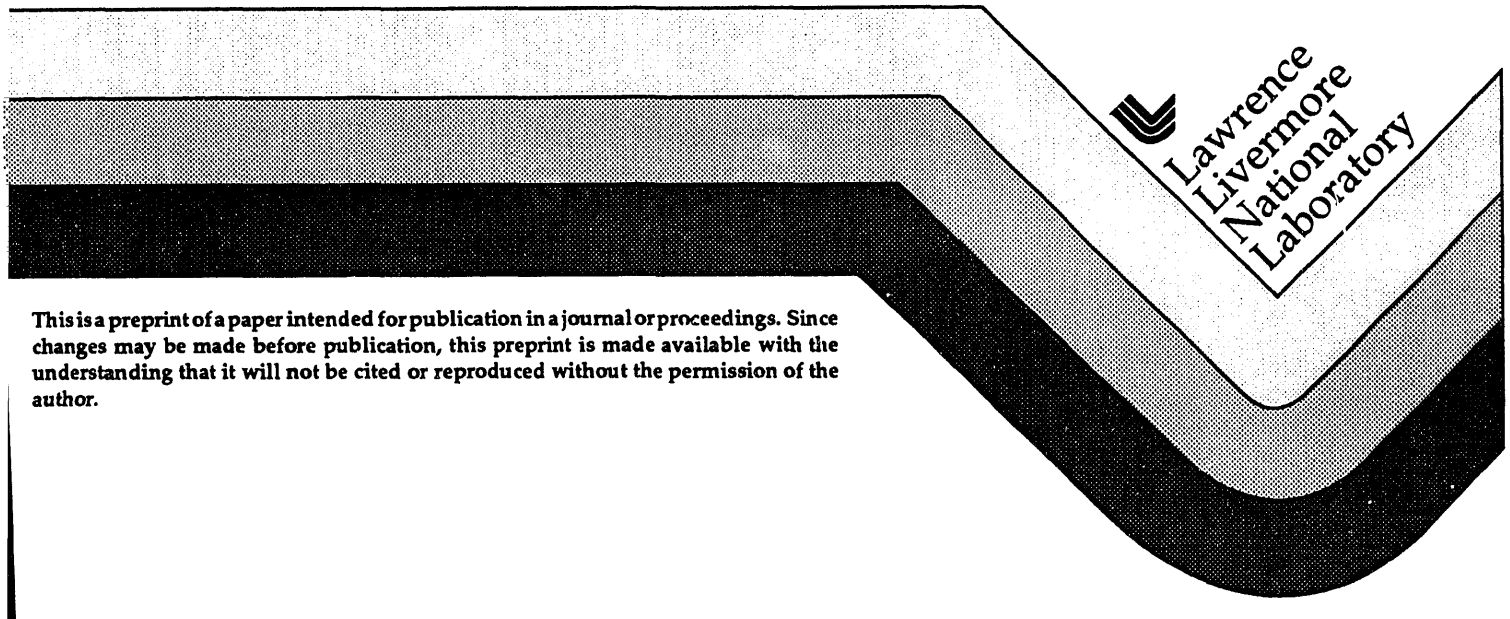

THE IMPACT OF REPOSITORY HEAT ON THERMO-HYDROLOGICAL PERFORMANCE AT YUCCA MOUNTAIN

Thomas A. Buscheck and John J. Nitao

Earth Sciences Department, L-206, P.O. Box 808

Lawrence Livermore National Laboratory, Livermore, CA 94551

telephone: (510) 423-9390, (510) 423-0297

ABSTRACT

To safely and permanently store high-level nuclear waste, the potential Yucca Mountain repository site must mitigate the release and transport of radionuclides for tens of thousands of years. In the failure scenario of greatest concern, water would contact a waste package (WP), accelerate its failure rate, and eventually transport radionuclides to the water table. Our analyses have demonstrated that the only significant source of liquid water is nonequilibrium fracture flow from: (1) meteoric sources, (2) condensate drainage generated under *boiling conditions*, and (3) condensate drainage generated under *sub-boiling conditions*. The first source of liquid water arises from the ambient system; the second and third sources are generated by repository heat. Buoyant vapor flow, occurring either on a sub-repository scale or on a mountain scale, may play an important role in the generation of the second and third sources of liquid water. By considering a wide range in bulk permeability, k_b, we identify the threshold k_b (called k_b^{hyd}) at which buoyant, vapor convection begins to dominate hydrological behavior, and the threshold k_b (called k_b^{th}) at which this convection begins to dominate thermal behavior. We find that k_b^{th} is generally an order of magnitude larger than k_b^{hyd} and that the development of a large above-boiling zone suppresses the effects of buoyant vapor flow. Zones of sharply contrasting k_b are also found to influence condensate generation and drainage. Of particular concern are conditions that promote the focusing of vapor flow and condensate drainage, which could result in persistent two-phase conditions (often referred to as the heat-pipe effect) in the vicinity of WPs. These effects can occur under both sub-boiling and boiling conditions. The results of this study underscore the need for *in situ* heater tests to help diagnose the potential for the major repository-heat-driven sources of fracture flow.

I. INTRODUCTION

The Yucca Mountain Site Characterization Project (YMP) of the U.S. Department of Energy (DOE) is investigating the suitability of the fractured, tuffaceous rocks occurring in the unsaturated zone (UZ) at Yucca Mountain, Nevada, for high-level nuclear waste storage. We have been examining repository-heat-driven hydrothermal flow in the UZ and saturated zone (SZ) at Yucca Mountain for a wide range of averaged thermo-hydrological properties, boundary conditions, and thermal loading conditions at the repository.[1-3] In the failure scenario of greatest concern, water would contact a waste package (WP), accelerate its failure rate, and eventually transport radionuclides to the water table. Our analyses have demonstrated that the only significant source of liquid water is from nonequilibrium fracture flow with three potential origins:

(1) meteoric sources,

(2) condensate generated under *boiling conditions*, and

(3) condensate generated under *sub-boiling conditions*.

The first source of liquid water arises from the ambient system; the second and third sources are generated by repository heat. Buoyant vapor flow, occurring either on a sub-repository scale or on a mountain scale (Figs. 1a and b), may play an important role in the generation of the second and third sources of liquid water. Zones of sharply contrasting bulk permeability, k_b, are also found to influence vapor and condensate flow, both under boiling and sub-boiling conditions. Of particular concern are conditions that promote the focusing of vapor flow and condensate drainage, which could cause persistent two-phase conditions in the vicinity of WPs (Fig. 1c). As shown later in this paper, repository heat can generate a mobile liquid phase in fractures even if temperatures are below the boiling point.

In addition to generating condensate flow, repository heat can redistribute the liquid saturation in the UZ, causing regions of net dry-out below the repository and saturation buildup above the repository. These changes can impact ambient fracture flow, possibly amplifying the effects of natural infiltration in regions of saturation buildup and attenuating those effects in regions of net dry-out. For high Areal Mass Loadings [(AMLs), expressed in metric tons of heavy initial metal per acre, MTU/acre)] that result in significant dry-out, mountain-scale, buoyant, vapor flow can also increase the rate at which the dry-out zone is re-wetted. Our repository-scale analyses[1-3] have indicated that repository-heat-driven changes in the saturation distribution can persist for more than 100,000 yr, even for low AMLs that never drive temperatures close to the boiling point.

It is important to note that our repository-scale analyses assume the repository thermal load to be uniformly distributed over a disk-shaped area with areally uniform thermo-hydrological properties. The vertical distribution of thermo-hydrological properties was included, assuming the major hydrostratigraphic units are horizontal. Effectively, the results of those calculations are representative of averaged, mountain-scale, thermo-hydrological behavior. In this paper, we examine how the spatial variability of heating conditions and hydrological properties may cause local thermo-hydrological behavior to deviate from averaged behavior. We also examine the conditions under which buoyant, vapor flow begin to dominate hydrological and thermal behavior for both sub-boiling and above-boiling thermal loads.

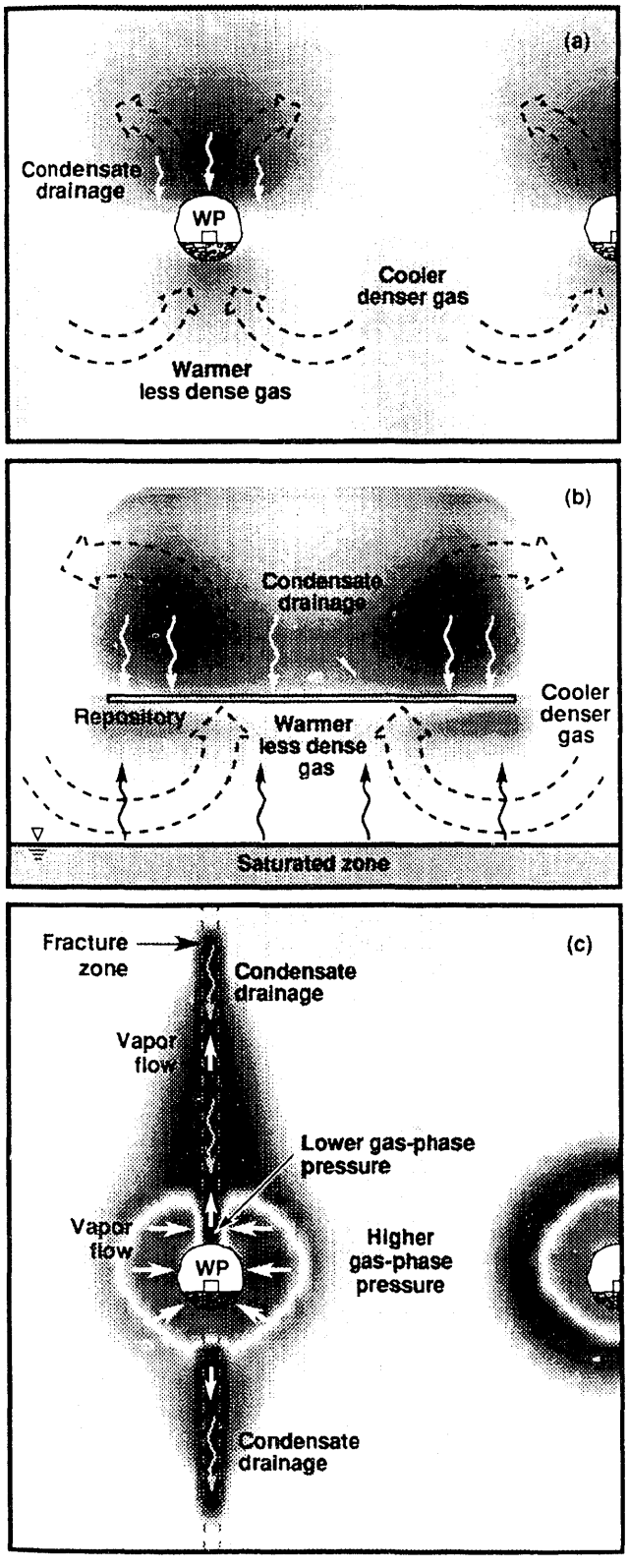

Figure 1. Model calculations of repository-heat-driven vapor and condensate flow. Buoyant vapor flow, occurring on either the (a) sub-repository scale or (b) mountain scale, drives moisture from below the repository to above, where it condenses. Condensate drains down fractures back toward the repository, and/or is imbibed by the matrix, possibly causing a saturation buildup above the repository. Water removed below the repository may be replenished by water imbibed from the SZ. (c) Zones of sharply contrasting bulk permeability, k_b, result in gas-phase pressure differentials that drive vapor flow into the high-k_b zone, where it condenses and drains, possibly causing persistant two-phase conditions in the vicinity of waste packages (WPs).

I.A Thermal Loading Strategies

The extent to which the three major sources of fracture flow may impact WP performance and radionuclide migration is critically dependent on ambient site conditions and as well as on the thermal loading strategy that will eventually be adopted for the Mined Geological Disposal System (MGDS) at Yucca Mountain. With respect to repository-heat-driven thermo-hydrological performance, there are three primary thermal loading strategies. These three strategies are best framed as three fundamental questions:

(1) Can the thermal load be limited and distributed such that it has a negligible impact on hydrological performance of the MGDS?

(2) For intermediate thermal loads, will the impact of thermo-hydrological processes and our understanding of those processes allow us to demonstrate that the MGDS meets regulatory compliance?

(3) For higher thermal loads, which have the potential of generating extended-dry conditions, will the impact of thermo-hydrological processes and our understanding of those processes allow us to demonstrate that the MGDS meets regulatory compliance?

The goal of the first thermal loading strategy is to minimize the hydrological impact of repository heat so that the primary concern in assessing hydrological performance is the ambient hydrological system. Therefore, this strategy requires that (1) we demonstrate that repository heat has a negligible impact on hydrological performance, and (2) the behavior of the ambient hydrological system and our understanding of that behavior are sufficient to demonstrate that the MGDS meets regulatory compliance. The motivation for this strategy is to avoid any potentially adverse effects of repository heat.

The goal of the third thermal loading strategy is to demonstrate that, for some period of time, repository heat is capable of dominating the ambient system with above-boiling conditions surrounding the repository. Ideally, this would result in (1) the absence of liquid water in the vicinity of the WPs as long as boiling persists, and (2) the continuation of sub-ambient liquid saturation conditions for some time following the above-boiling period without incurring adverse effects that may offset the benefits of dry-out. The primary motivations for this strategy are to (a) minimize the sensitivity of repository

performance to hydrological variability, (b) extend the period of radionuclide containment in the engineered barrier system, and, (c) during the period of radionuclide migration, reduce two factors: the probability of water contacting WPs and the flow rates associated with transport. Another important motivation is to delay the period of significant radionuclide migration until the inventory of radionuclides has been substantially diminished by radioactive decay.

The second thermal loading strategy falls between the first and third strategies. All three strategies require an adequate understanding of both the ambient hydrological system and how heat perturbs fluid flow in that system.

It is important to note that what effectively constitutes a "cold" ambient-system-dominated repository or a "hot" extended-dry repository is not well understood. Presently, we lack adequate knowledge of ambient site conditions to define where the transitions from cold to intermediate or from intermediate to hot thermal loads occur. In this paper, we analyze how site conditions will influence the determination of these transitions. In particular, the influence of buoyant, gas-phase convection and how hydrogeological heterogeneity may focus vapor and condensate flow are critical to determining what thermal loads are sufficiently "cold" to render hydrothermal impacts of repository heat as negligible. The influence of these processes will also largely determine what thermal loads are sufficiently "hot" (or whether any such thermal loads exist) to allow us to demonstrate that extended-dry conditions will prevail for some time in the vicinity of WPs.

Generally speaking, site conditions that are beneficial to a "cold" repository also benefit the performance of a "hot" repository. If we find that k_b is too small to promote significant buoyant, gas-phase flow and that the contrast in k_b between neighboring zones is insufficient for significant focusing of vapor flow and condensate drainage, it may be possible to demonstrate that a sub-boiling repository has a negligible impact on the ambient hydrological system. These same site conditions are also beneficial to extending the period of above-boiling temperatures and, during that time, minimizing the presence of mobile liquid water in the vicinity of WPs.

I.B Overview of UZ Hydrology at Yucca Mountain

Yucca Mountain consists of a series of variably fractured, nonwelded to densely welded tuff units with an eastward tilt of 5 to 30 deg.[4] The UZ thickness varies from 500 to 750 m. The potential repository location is in Topopah Spring (TSw2) moderately to densely welded tuff, which is about 350 m below the ground surface and 225 m above the water table.[5] Montazer and Wilson report the absence of perennial streams at Yucca Mountain.[4] Therefore, recharge due to rainfall or snowmelt occurs episodically.

The matrix properties of the hydrostratigraphic units at Yucca Mountain are summarized by Klavetter and Peters.[5] The units generally fall into two categories: (1) the welded tuffs (TCw, TSw1, TSw2, and TSw3) and the nonwelded zeolitized unit (CHnz), all of which have low matrix permeability, k_m, and low-to-medium matrix porosity, ϕ_m, and (2) nonwelded vitric tuffs of high k_m and ϕ_m (PTn and CHnv). The welded PPw has medium k_m and ϕ_m. The values of k_m in the nonwelded vitric tuffs are 4 to 5 orders of magnitude greater than those of the welded tuffs and the CHnz.

Infiltration at Yucca Mountain has been modeled with a one-dimensional steady-state equivalent continuum model (ECM) for recharge fluxes of 0, 0.045, and 0.132 mm/yr, resulting in repository horizon saturations of 68, 85, and 95%, respectively.[6] On the basis of the assumption of instantaneous capillary pressure equilibrium between fracture and matrix, the ECM volume-averages the fracture and matrix into an equivalent (or effective) continuum. Saturation values obtained from the Reference Information Base (RIB)[7] agree with the saturation profile calculated for zero recharge flux in the low-k_m units (TCw, TSw1, TSw2, TSw3, CHnz, and PPw). The RIB values were significantly higher than the calculated profile for the high-k_m units (PTn and CHnv). Nonequilibrium fracture flow through the TCw, TSw1, TSw2, and TSw3 is a likely cause for the apparent inconsistency between the RIB data in the PTn and CHnv and the saturation profile predicted by the one-dimensional, steady-state ECM.[6]

Numerous performance assessment calculations have been carried out for the potential Yucca Mountain repository site. Most of these have utilized a steady-state ECM that, for the assumed recharge fluxes, effectively constrains flow to be matrix-dominated.[6,8] Because of the very low k_m prevalent through most of the UZ, the steady-state ECM calculations have repeatedly shown that matrix-dominated flow will not result in significant vertical transport of radionuclides. Moreover, field evidence indicates that nonequilibrium fracture flow can occur to considerable depth.[9] Therefore, nonequilibrium fracture flow is the only credible mechanism capable of bringing water to the WPs and transporting radionuclides to the water table.

I.C Hydrothermal Flow at the Repository Horizon

Much of our current understanding of repository-heat-driven hydrothermal flow in unsaturated fractured tuff is based on observations made during the heater tests in G-Tunnel[10] and associated modeling studies.[11,12] For drift emplacement without backfill, the primary mode of heat transfer from the WP to the wall of the emplacement drift is thermal radiation (Fig. 2). If backfill is present, heat flow through the backfill will be dominated by heat conduction.

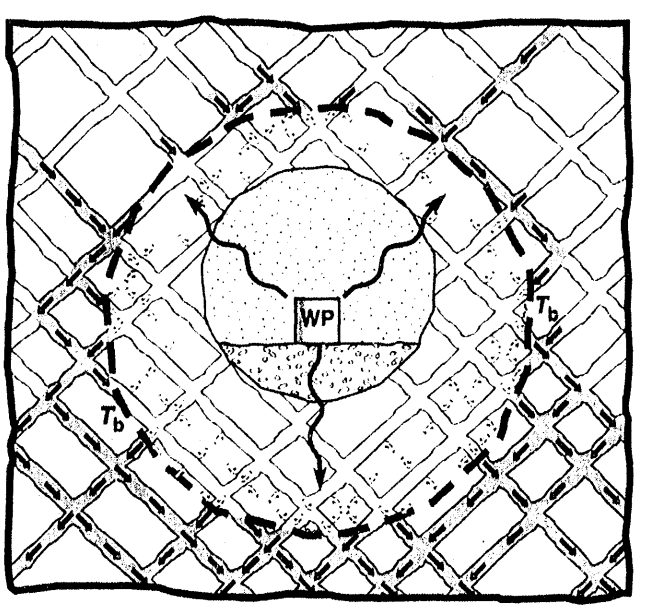

Figure 2. Schematic of hydrothermal flow near the emplacement drift. Rock dry-out occurs as boiling drives water vapor out of the rock matrix. Upon reaching the fracture network, vapor is driven away from the boiling zone to where cooler temperatures cause it to condense along fracture walls. Because the small k_m limits the rate of matrix imbibition, condensate drainage persists for considerable distances down fractures.

Both the G-Tunnel heater test modeling analysis[12] and subsequent analyses of repository-heat-driven hydrothermal flow[1-3] have indicated that heat flow in the UZ is likely to be dominated by heat conduction. Because of the large bulk permeability, k_b, of fracture networks, gas-phase pressures, p_g, in the fractures remain very close to atmospheric, even during boiling. Consequently, as temperatures reach the nominal boiling point ($T_b \approx 96°C$), boiling first occurs along the fracture faces, i.e., the perimeter of the matrix blocks, and proceeds in toward the center of the matrix blocks. Because of the small k_m at the repository horizon, boiling results in large p_g gradients (with p_g increasing from the perimeter to the center of the matrix blocks), causing a rise in the boiling temperature, ΔT_b, above the nominal boiling point, T_b. Because p_g gradients increase with matrix block size, ΔT_b increases with matrix block size. Accordingly, boiling is more suppressed in sparsely fractured regions and less suppressed in intensely fractured regions. For regularly spaced fractures, the volume of the dry-out zone was found to be proportional to $\sqrt{k_m}/B$, where B is the effective fracture spacing.[12] For the G-Tunnel test, B was apparently small enough (relative to k_m) that the effect of ΔT_b on rock dry-out was negligible. The sensitivity of the dry-out volume to fracture aperture, b, was also examined.[12] Assuming three fractures per meter, we found for $b > 20$ μm that the volume of the dry-out zone is insensitive to b. For three 20-μm fractures per meter, the equivalent k_b is 2.4 millidarcy. Similarly, our analysis of repository-heat-driven flow[3] indicated that for high AMLs, dry-out due to boiling is effectively not throttled for $k_b > 1$ millidarcy (equivalent to three 15-μm fractures per meter).

At early time, a small percentage of the water vapor that reaches the fractures in the immediate vicinity of the WP flows back toward the emplacement drift (Fig. 2). Otherwise, most of the water vapor reaching the fracture network is driven away from the emplacement drift by higher gas-phase pressures in the boiling zone to where cooler temperatures cause it to condense along fracture walls. For sufficiently large k_b, gas-phase pressures in the boiling zone will not be large enough to oppose the effects of thermal gas-phase buoyancy. As buoyant, gas-phase convection develops, water vapor that is within fractures pneumatically connected to the buoyant convective system will tend to move upward to where cooler temperatures cause it to condense along fracture walls.

The generalization that water vapor is preferentially driven away from the emplacement drift does not necessarily hold for heterogeneously fractured rock, which contains zones of sharply contrasting k_b. Later in this paper, we analyze cases in which the drift is intersected by such zones. We find that if the contrast in k_b between the high-k_b zone and the rest of the rock surrounding the drift (called the nominal-k_b zone) is sufficiently large, then the p_g differential between these zones will drive water vapor back toward the drift and into the high-k_b zone (Fig. 1c). In effect, the emplacement drift functions as a manifold that enhances the gas-phase communication between the high- and nominal-k_b zones. If enough water vapor is focused into the high-k_b zone, then the resulting condensate generation and drainage back down that zone may result in persistent two-phase conditions at the edge of the drift and water dripping onto the WPs.

In general, regardless of where it is generated, there are three things that can happen to the condensate:

(1) It can drain away from the boiling zone.

(2) It can drain back toward the boiling zone.

(3) It can be imbibed by the matrix.

Because the small k_m limits the rate of matrix imbibition, condensate drainage down fractures persists for considerable distances before being imbibed by the matrix. Below the boiling zone, condensate drainage is away from the boiling zone (Fig. 2), enhancing the dry-out rate. Above the boiling zone, condensate tends to drain back toward the boiling zone, where it reboils, thereby retarding the net rate of dry-out. Until boiling reduces the liquid saturation to zero, temperatures will be determined by two-phase thermodynamic equilibrium. The effect of vapor pressure lowering (which results from surface forces between the water and the matrix) can make it difficult to reduce the liquid saturation in the matrix to zero even though temperatures may be well above the nominal boiling point. Under such conditions, the fractures are likely to be completely free of *mobile* liquid water. Immobile water, tightly held by surface forces, may be present in the rock at temperatures above the boiling point. An important question is whether, as a result of heterogeneous fracture connectivity, enough water vapor and condensate can be focused into a local region of the repository to locally collapse the zone of above-boiling temperatures.

II. NUMERICAL MODELS AND ASSUMPTIONS

II.A V-TOUGH Hydrothermal Flow Code

All hydrothermal calculations were carried out using the V-TOUGH (vectorized transport of unsaturated groundwater and heat) code.[13] V-TOUGH is Lawrence Livermore National Laboratory's enhanced version of the TOUGH code, which is a member of the Mulkom family of multiphase, multicomponent codes developed at Lawrence Berkeley Laboratory by Pruess.[14] V-TOUGH is a multidimensional numerical simulator capable of modeling the coupled transport of water, vapor, air, and heat in fractured porous media.

II.B Equivalent Continuum Model

Because of the impracticality of discretely accounting for all of the fractures at Yucca Mountain, it was necessary to account for fractures using the ECM. The assumption of capillary pressure and thermal equilibrium between fractures and matrix allows the fracture and matrix properties to be pore-volume-averaged into an equivalent medium. The bulk porosity, ϕ_b, bulk saturation, S_b, and bulk hydraulic conductivity, K_b, of the equivalent medium are given by:

$$\phi_b = \phi_f + (1-\phi_f)\phi_m \tag{1}$$

$$S_b = \frac{S_f\phi_f + S_m(1-\phi_f)\phi_m}{\phi_f + (1-\phi_f)\phi_m} \tag{2}$$

$$K_b = K_m(1-\phi_f) + K_f\phi_f \tag{3}$$

where ϕ_m, S_m, ϕ_f, and S_f are the porosity and saturation of the matrix and fractures, respectively, and K_m and K_f are the hydraulic conductivities of the matrix and fractures. Because of the small K_m in the UZ, K_b is almost completely dominated by K_f and ϕ_f for most fracture spacings and permeabilities.

II.C Thermo-Hydrological Properties

All major hydrostratigraphic units in the UZ at Yucca Mountain are included in the models.[5,15] The hydrostratigraphic profile employed here has been used in previous modeling studies.[1-3] The wet and dry thermal conductivity, K_{th}, data were obtained from the RIB.[7] We assume the steady-state liquid saturation profile obtained for a net recharge flux of 0 mm/yr, yielding a repository horizon saturation of 68%.[6] Previous work[1-3] also considered the steady-state saturation profile obtained for recharge fluxes of 0.045 and 0.132 mm/yr, resulting in repository saturations of 85 and 95%, respectively.

The reference case assumed a bulk permeability, k_b, of $2.8 \times 10^{-13} m^2$ (280 millidarcy), which is equivalent to three 100-μm

fractures per meter. The sensitivity of buoyant, gas-phase convection, boiling and dry-out performance to k_b was examined by considering the following values of k_b: 1.9 microdarcy (no fractures), 10 microdarcy (three 3-μm fractures per meter), 100 microdarcy (three 7-μm fractures per meter), 1 millidarcy (three 15-μm fractures per meter), 10 millidarcy (three 33-μm fractures per meter), 1 darcy (three 153-μm fractures per meter), 5 darcy (three 262-μm fractures per meter), 10 darcy (three 330-μm fractures per meter), 20 darcy (three 416-μm fractures per meter), 40 darcy (one 781-μm fracture per meter), 84 darcy (one 1000-μm fracture per meter), 168 darcy (one 1260-μm fracture per meter), 414 darcy (one 1700-μm fracture per meter), and 840 darcy (one 2150-μm fracture per meter).

II.D Initial and Boundary Conditions

The vertical temperature distribution, T, in the models is initialized to correspond to the nominal geothermal gradient in the region. The atmosphere at the ground surface is represented by a constant-property boundary, with T and p_g fixed at 13°C and 0.86 atm, respectively. The relative humidity at the ground surface is also fixed so that it is in thermodynamic equilibrium with the initial saturation conditions at the top of the TCw unit. Therefore, under initial (ambient) saturation and temperature conditions, there is no mass flux of water vapor between the atmosphere and upper TCw. In previous work,[1] it was assumed that because of the large fracture permeability, buoyant convective mixing in the SZ results in it acting as a heat sink. The large k_b and storativity of the SZ were also assumed to result in the water table being at a fixed depth. For the drift-scale calculations reported here, we also assume that the water table has a fixed depth ($z = 568.1$ m) and a constant temperature (31°C). The constant-temperature water table assumption causes the water table to act as a heat sink. Because this model does not explicitly model hydrothermal flow in the SZ, it is called the "UZ" model. In comparing the UZ model with the UZ-SZ model, which is described below, we found that, for the first 1000 yr, repository temperatures are insensitive to the treatment of heat flow at the water table.[2,3] Because the primary use of the drift-scale model is to examine sub-repository-scale, thermo-hydrological behavior during the first 1000 yr, the constant-temperature water table assumption does not significantly affect the interpretation of our results. The initial temperature and saturation at the repository horizon in the UZ model are 23.3°C and 68%, respectively.

We conduct most of our calculations with a UZ-SZ model (which includes hydrothermal flow in the upper 1000 m of the SZ). Conductive and convective heat flow, including buoyancy flow, are modeled in the SZ. Because the RIB[7] lacks thermal property and hydrological data below the PPw unit (the lowermost hydrostratigraphic unit in our UZ model), we assumed that the PPw data was applicable to the upper 1000 m of the SZ (down to the lower boundary of the UZ-SZ model). The lower boundary of the UZ-SZ model has a constant temperature of 53.5°C and a fixed pressure corresponding to the hydrostatic pressure and temperature profile of the upper 1000 m of the SZ. The initial temperature and saturation at the repository horizon in the UZ-SZ model are 23.5°C and 67.7%, respectively.

II.E Repository-Scale Model

For the reference thermal load, given by the Site Characterization Plan–Conceptual Design Report[16] (SCP-CDR), with 10-yr-old SNF and an Areal Power Density (APD) of 57 kW/acre (yielding an AML of 49.2 MTU/acre), we assumed that the heated area of the repository is 1747 acres. For a 1747-acre repository, the repository-scale model represents the repository as a 3-km-diameter, 4.6-m-thick, disk-shaped heat source with a uniformly distributed thermal load. Repository areas of 559, 1118, and 3162 acres were also modeled for AMLs of 154.7, 77.3, and 27.1 MTU/acre, respectively. The model utilizes an axisymmetric coordinate system centered at the repository center. This model is useful for calculating temperature and saturation behavior (averaged from one emplacement drift to the next) as a function of location relative to the center (or edge) of the repository area. The assumption was also made that the thermal loading of the repository can be represented by the heat generation curve of pressurized water reactor (PWR) spent nuclear fuel (SNF) of an average age. Calculations were made for APDs ranging from 10 to 114 kW/acre and SNF ages of 10, 20, and 30 yr with a burnup of 33,000 MWd/MTU.

II.F Sub-Repository-Scale Models

Because it areally averages the thermal load, the repository-scale model cannot represent differences in temperature and saturation behavior within (1) the pillars (i.e., the rock separating neighboring emplacement drifts), (2) the emplacement drifts, or (3) the WPs themselves. The drift-scale model is a two-dimensional cross-sectional model that explicitly represents the details of the WPs and emplacement drifts in the plane orthogonal to the drift axes. This model is useful in representing details of thermo-hydrological behavior at the drift (or sub-repository) scale. In particular, we are interested in how sub-repository-scale, buoyant, gas-phase convection (which is driven by temperature differences between the drifts and pillars) affects vapor and condensate flow and thermal performance. To take advantage of symmetry, the drift-scale model assumes an infinite repository with uniformly spaced emplacement drifts. The assumption of an infinite repository area is applicable to the interior of the repository that is not affected by cooling at the edge. This region includes most of the repository area during (at least) the first 1000 yr.

The drift-scale model assumes the 38.4-m center-to-center spacing between emplacement drifts that is found in the SCP-CDR.[16] The model represents a symmetry element from the symmetry plane down the center of the WP to the symmetry plane in the pillar between neighboring drifts. The thermal load is axially averaged along the axis of the drift. The WP has a cross section of 1.6 x 1.6 m and is located in the center of an emplacement drift that is 4.8 m high by 6.0 m wide. The drifts are assumed to remain open; therefore, heat flow from the WP surface to the drift wall occurs as thermal radiation, convection, and conduction. The drift-scale model can represent heterogeneity that occurs at the scale of the drifts. For some of our calculations, a 1.6-m-wide, high-k_b zone is oriented vertically, parallel to the WP axis. The k_b of this zone can be several orders of magnitude larger than k_b throughout the rest of the model (the nominal-k_b zone). The center-to-center spacing between the high-k_b zones is 38.4 m (the same as the center-to-center drift spacing).

Heterogeneity that occurs at a larger scale is represented by a third model, which we call the cross-sectional uniform heat flow (CSUHF) model. Like the drift-scale model, the CSUHF model assumes an infinite repository, thereby enabling it to take advantage of symmetry. The CSUHF model represents an infinite series of vertical, uniformly-spaced, 1.0-m-wide, high-k_b zones. We considered high-k_b zone spacings of 100 and 1000 m. For the high-k_b zones, we considered 10, 84, 414, and 840 darcy. For the nominal-k_b zones, we considered 1.9 and 100 microdarcy; 1, 10, 100 and 280 millidarcy; and 10 darcy.

III. DISCUSSION OF MODEL RESULTS

As in other studies,[1-3] we have utilized idealizations of (1) the repository thermal load, (2) the distribution of thermo-hydrological properties, and (3) boundary and initial conditions. No individual

model of the repository-UZ-SZ system is itself a "valid" representation; however, the combined use of various models, and the consideration of broad ranges in parameters, provides a means to identify critical dependencies, evaluate worst-case scenarios, and develop hypotheses, which can be addressed by subsequent analysis and testing. Pruess and Tsang[17] have shown that through the complementary use of models, the limitations of a particular model can be partially overcome, providing increased confidence for predictions. Our view has been that of Konikow and Bredehoeft,[18] who believe that the process of model validation must involve developing and performing critical sets of analyses and experiments in an attempt to test, or invalidate, a model (or hypothesis).

As in past studies,[1-3] we examine the sensitivity of thermo-hydrological behavior to thermal loading design parameters, thermo-hydrological properties, and boundary conditions. A broad range of parameters and conditions are investigated to identify distinct regimes of thermo-hydrological performance, particularly as they affect the following hypothesis tests:

(1) whether heat conduction dominates heat flow,

(2) whether a region of above-boiling temperatures surrounding the repository corresponds to the absence of *mobile* liquid water at the WP environment,

(3) whether fracture density and connectivity are sufficient to promote rock dry-out due to boiling and condensate shedding,

(4) whether re-wetting of the dry-out zone back to ambient saturation lags significantly behind the end of the boiling period,

(5) whether mountain-scale, buoyant, gas-phase convection may eventually dominate moisture movement in the UZ,

(6) whether sub-repository-scale, buoyant, gas-phase convection dominates moisture movement at the repository, and

(7) whether heterogeneity results in focusing enough vapor flow and condensate drainage to cause persistent local liquid flow at the WP environment.

Demonstrating that the first two hypotheses are *true* is very favorable for performance during the above-boiling period. If conduction dominates heat flow, the adequacy of heat flow models will depend primarily on accurate accounting of the thermal properties and thermal loading conditions, which are more readily determined and much less variable than many parameters of the ambient hydrogeological system. Moreover, the thermal properties are relatively insensitive to hydrothermally driven geochemical effects. The range of RIB[12] values of thermal conductivity at Yucca Mountain only spans a factor of 2. If conduction dominates heat flow, then we should be able to reliably predict the region of above-boiling conditions surrounding the repository. Demonstrating that the second hypothesis is *true* favors performance because the absence of *mobile* water benefits WP integrity and eliminates advective liquid flow as a mechanism for mobilizing and transporting radionuclides.

Demonstrating that the first four hypotheses are *true* is favorable for post-boiling period performance, which benefits from a persistent zone of sub-ambient saturations surrounding the repository. The first three hypotheses provide the basis for reliably predicting the spatial extent of the dry-out zone surrounding the repository. The fourth hypothesis provides the basis for predicting how long the dry-out zone persists. Demonstrating that hypotheses (5) through (7) are *false* is favorable for both above-boiling and sub-boiling performance. By showing that hypotheses (5) and (6) are *false*, we will eliminate a major potential source of fracture flow, particularly for sub-boiling conditions, as well as a potential mechanism for building up the saturation above the repository and re-wetting the dry-out zone. By showing that hypothesis (7) is *false*, we will eliminate a major potential source of fracture flow for both sub-boiling and above-boiling conditions.

It is critically important to resolve hypotheses (1), (5), (6), and (7) even if temperatures never exceed the boiling point. As discussed in Section III.A, mountain-scale, buoyant, gas-phase convection will dominate heat flow only for a very large vapor flux that results in a large saturation buildup above the repository and/or a large condensate drainage flux in fractures. Therefore, hypotheses (1) and (5) are extremely important for all AMLs. As discussed in Section III.B, it is critically important to resolve hypothesis (6), particularly for a thermal loading strategy that relies on a sub-boiling thermal load having a negligible impact on hydrological performance. As discussed in Section III.C, hypothesis (7) is important for all AMLs, because focused vapor and condensate flow can cause persistent liquid flow at the WP environment for both sub-boiling and boiling conditions.

III.A Mountain-Scale, Buoyant, Gas-Phase Flow

We used the repository-scale, UZ-SZ model to study the thermo-hydrological impact of mountain-scale, buoyant, gas-phase flow over a wide range of k_b and AML, including 27.1, 49.2 (the reference SCP-CDR thermal load), and 154.7 MTU/acre. We started by assuming a homogeneous and isotropic k_b distribution in the UZ and SZ. Later in this section, we consider the impact of a layered, heterogeneous k_b distribution. Because the matrix permeability is so small for most of the UZ, differences in k_b reflect differences in fracture permeability.

Mountain-scale, buoyant, gas-phase convection occurs within fracture networks having a connectivity with length scale comparable to the UZ thickness and repository width (Fig. 1b). Buoyant gas-phase convection cells develop as the warmer, less dense column of gas within the footprint of the repository is displaced by the cooler, denser column of gas outside of the repository footprint. As the initially cooler gas is heated up, its relative humidity is lowered, causing it to evaporate water from the rock matrix below the repository. This warm moist air is convected upward to where it cools above the repository, generating condensate that drains down fractures back toward the repository and/or is imbibed by the matrix, causing a saturation buildup above the repository. Because water removed below the repository may be replenished by water imbibed from the SZ, this process can result in a net saturation buildup in the UZ. We find that mountain-scale, buoyant, vapor flow can dominate moisture movement on the order of 100,000 yr.

For an AML of 27.1 MTU/acre (30-yr-old SNF and an APD of 20 kW/acre), we considered the following values of k_b: 280 millidarcy and 10, 20, 40, 84, 168, 414, and 840 darcy. An AML of 27.1 MTU/acre results in a T_{peak} of 60°C at the center of the repository (Fig. 3a), regardless of k_b. Depending on the number of SNF assemblies per WP, local boiling conditions may persist for some time even though average temperatures are well below boiling. For k_b<10 darcy, mountain-scale, buoyant, gas-phase convection does not result in a net change to the liquid saturation distribution; however, significant refluxing occurs, with buoyant vapor flow being balanced by condensate drainage and imbibition. For k_b>10 darcy, condensate drainage and imbibition cannot keep up with buoyant vapor flow, and regions of net dry-out below the repository and condensate buildup above the repository develop and persist for tens of thousands of years. With the ECM, we cannot determine whether this condensate flux results in nonequilibrium fracture flow down to the repository

horizon (and possibly down to the water table). However, the potential for nonequilibrium condensate drainage exists even for situations that do not result in a net redistribution of liquid saturation. Large-scale *in situ* heater tests, conducted under both sub-boiling and above-boiling conditions, are needed to determine the potential for mountain-scale, buoyant, vapor flow to drive nonequilibrium condensate drainage in the vicinity of WPs.[19,20]

On the basis of the ECM and a uniform k_b distribution, we find, for an AML of 27.1 MTU/acre, that the threshold k_b (called k_b^{hyd}) at which mountain-scale, buoyant, gas-phase convection results in net changes to the liquid saturation distribution is approximately 10 darcy. For a model that explicitly treats nonequilibrium fracture flow, k_b^{hyd} may be different. We find that the threshold k_b (called k_b^{th}) at which buoyant convection begins to dominate thermal performance is 10 times larger than k_b^{hyd}. For an AML of 27.1 MTU/acre and k_b=84 darcy, we find that buoyant vapor flow begins to noticeably affect temperatures in the far-field and at the edge of the repository, but not at the repository center (Fig. 3a). For k_b = 168 darcy, buoyant vapor flow dominates far-field temperatures, significantly reduces temperatures at the repository edge, and begins to affect temperatures at the repository center. In general, mountain-scale, buoyant, gas-phase convection does not influence temperatures at the repository center until after they peak ($t_{peak} \approx 600$ yr).

The order-of-magnitude difference between k_b^{hyd} and k_b^{th} indicates that, for the hydrological (buoyant gas-phase) flow system to dominate repository-generated heat flow, the latter must have had a dominant impact on the hydrological flow system, including both liquid-phase and gas-phase flow. Furthermore, the thermal impacts of mountain-scale, buoyant, gas-phase convection occur earlier and more readily (and are more pronounced) in the far-field than at the repository. In general, we will always know more about repository temperatures than about any other aspect of thermo-hydrological performance. Moreover, the magnitude of buoyant convective effects required to dominate repository thermal performance will be associated with a dramatic increase in liquid saturation above the repository, possibly resulting in significant condensate drainage at the repository horizon (and to the water table). A major issue that can be addressed by large-scale, above-boiling, *in situ* heater tests,[19,20] is whether conduction or convection dominates the thermal performance of the repository.

We also considered cases in which the distribution of k_b varies vertically, which results in a layered distribution. This was done in consideration of the unpublished k_b data of Weeks,[21] which indicates considerable layering of k_b. In particular, it appears that k_b may be far smaller in the nonwelded vitric units (PTn and CHnv) and the nonwelded zeolitized CHnz than in the welded units (TCw, TSw1, TSw2, and TSw3). For an AML of 27.1 MTU/acre, we considered a case in which k_b=84 darcy everywhere in the UZ except in the PTn, where k_b= 320 millidarcy. For the case in which k_b=84 darcy throughout the UZ, mountain-scale, buoyant, gas-phase convection behaves as though it is in an "open" system with respect to the ground surface. In this open system, the gas-phase velocity vectors are orthogonal to the ground surface in the vicinity of the ground surface. Buoyant vapor flow results in a substantial increase in liquid saturation from the repository horizon all the way to the ground surface. In the case in which k_b= 320 millidarcy in the PTn, this unit functions as a gas-phase flow barrier or "vapor cap." Consequently, the direction of gas-phase flow below the PTn/TSw1 contact becomes tangential to this contact rather than crossing the PTn. The PTn effectively isolates the buoyant, gas-phase, convection cells from the ground surface, thereby causing the convective system be "closed" with respect to the ground surface. The magnitude of buoyant, gas-phase flow and saturation alteration in the "closed" convective system is nearly three times less than in the "open" convective system.

In general, hydrostratigraphic units (e.g., the PTn) that are found to have a substantially smaller k_b can function as "vapor caps" limiting the vertical extent and magnitude of repository-heat-driven saturation alteration. The role of the PTn in limiting these effects may prove to be more significant than its impact on the infiltration of meteoric water.

We continue the analysis of cases with a uniform k_b throughout the UZ. For the reference SCP-CDR thermal load (an AML of 49.2 MTU/acre, 10-yr-old SNF, and an APD of 57 kW/acre), we considered the following values of k_b: 280 millidarcy and 1, 5, 10, 20,

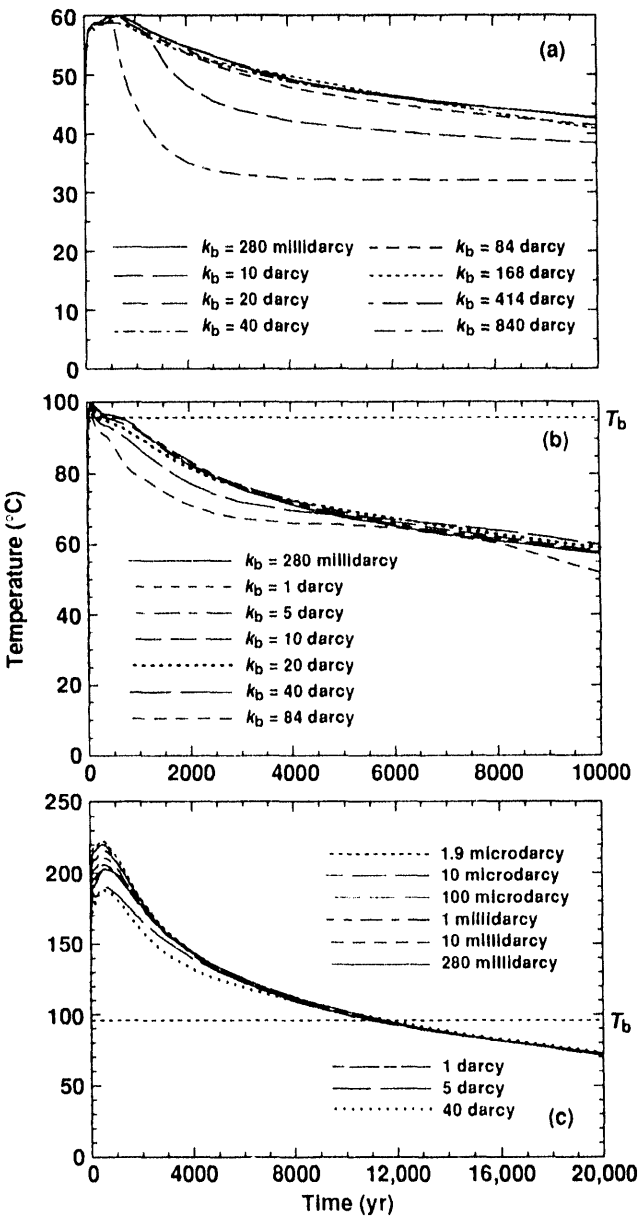

Figure 3. Temperature history at repository center for a net recharge flux of 0 mm/yr, including hydrothermal flow in the SZ. (a) For 30-yr-old SNF, an AML of 27.1 MTU/acre, and an APD of 20 kW/acre. (b) For 10-yr-old SNF, an AML of 49.2 MTU/acre, and an APD of 57 kW/acre. (c) For 30-yr-old SNF, an AML of 154.7 MTU/acre, and an APD of 114 kW/acre. Note the different time scales.

40, and 84 darcy. For $k_b = 1$ darcy, mountain-scale, buoyant, gas-phase convection has a minor effect on temperatures, reducing the duration of the boiling period at the repository center, t_{bp}, from 666 to 618 yr relative to the 280-millidarcy case (Fig. 3b). Although it has minor effect on temperatures, buoyant convection does significantly impact moisture movement, driving significant quantities of vapor from below the repository to above, where it condenses. For $k_b \geq 1$ darcy, condensate drainage cannot keep up with buoyant vapor flow, and regions of net dry-out below the repository and net condensate buildup above it develop and persist for tens of thousands of years. Therefore, k_b^{hyd} is in the range of 1 to 5 darcy. For the 10-darcy case, mountain-scale, buoyant, gas-phase convection reduces t_{bp} from 666 to 417 yr; whereas, for the 20-darcy case, the thermal impact becomes quite substantial, reducing t_{bp} from 666 to 242 yr (Fig 3b). Therefore, k_b^{th} is about 20 darcy. The thermal impact is even more pronounced for the 40-darcy case, in which t_{bp} is reduced from 666 to only 173 yr relative to the 280-millidarcy case.

The effect that mountain-scale, buoyant, gas-phase flow may have on altering the liquid saturation distribution in the UZ and its dependence on k_b is shown in Fig. 4. For this example (AML = 49.2 MTU/acre), dry-out due to boiling peaks at about $t = 300$ yr. Any dry-out that occurs after the boiling period ($t > t_{bp}$) is driven by mountain-scale, buoyant, gas-phase convection. Note that t_{bp} is 666, 417, and 116 yr for the cases represented in Figs. 4a–c, respectively. For the 280-millidarcy case (Fig. 4a), the dry-out zone has re-wetted back to ambient conditions within 10,000 yr, and mountain-scale, buoyant, gas-phase convection has a negligible impact on the saturation distribution. For the 10-darcy case (Fig. 4b), mountain-scale, buoyant, vapor flow has resulted in a substantial buildup in saturation over a vertical interval that includes the repository horizon. Note that, because water removed below the repository can be replenished by water imbibed from the SZ, the volume of condensate buildup greatly exceeds the dry-out volume. For the 84-darcy case (Fig. 4c), this buildup in condensate causes the liquid saturation to approach 100% over a large vertical interval. The saturation profiles shown in Figs. 4b and c require more than 100,000 yr to re-equilibrate back to ambient conditions.

For an AML of 154.7 MTU/acre (30-yr-old SNF and an APD of 114 kW/acre), Fig. 3c shows the temperature at the repository center for the following values of k_b: 1.9, 10, and 100 microdarcy; 1, 10, and 280 millidarcy; and 1, 5, and 40 darcy. Notice that t_{bp} is insensitive to k_b over this 7 orders of magnitude range in k_b. In a previous study,[1] repository temperatures were found to be insensitive to k_b over the range 1.9 microdarcy $< k_b <$ 10 darcy for an AML of 77.4 MTU/acre. Repository-driven heat flow is effectively conduction-dominated over that range. Notice that T_{peak} is modestly sensitive to k_b, decreasing slightly with increasing k_b (Fig. 3c). The modest dependence of T_{peak} on k_b is related to the vertical extent of dry-out due to boiling. With no fractures, there is no dry-out because the small matrix permeability results in large gas-phase pressures, causing a rise in the boiling temperature, ΔT_b, which suppresses boiling. The absence of convective and boiling effects in the 1.9-microdarcy case results in conduction-dominated heat flow and a higher T_{peak} (222.1°C) than in the 280-millidarcy case (202.9°C).

Mountain-scale, buoyant, gas-phase convection has a negligible effect on thermal performance for the 5-darcy case (Fig 3c). It also has a negligible effect on thermal performance at the repository center for the 40-darcy case, with $t_{bp} = 11{,}500$ yr for both the 40-darcy and 280-millidarcy cases. Also notice that T_{peak} is virtually the same for the 5-darcy case (190.0°C) and the 40-darcy case (187.4°C). Because buoyant gas-phase convection already drives 100% of the steam above the dry-out zone for the 5-darcy case, increasing k_b above 5 darcy does not have the effect of driving additional moisture to the upper condensation zone. Therefore, the upward flow of steam through the center of the repository is not significantly enhanced in

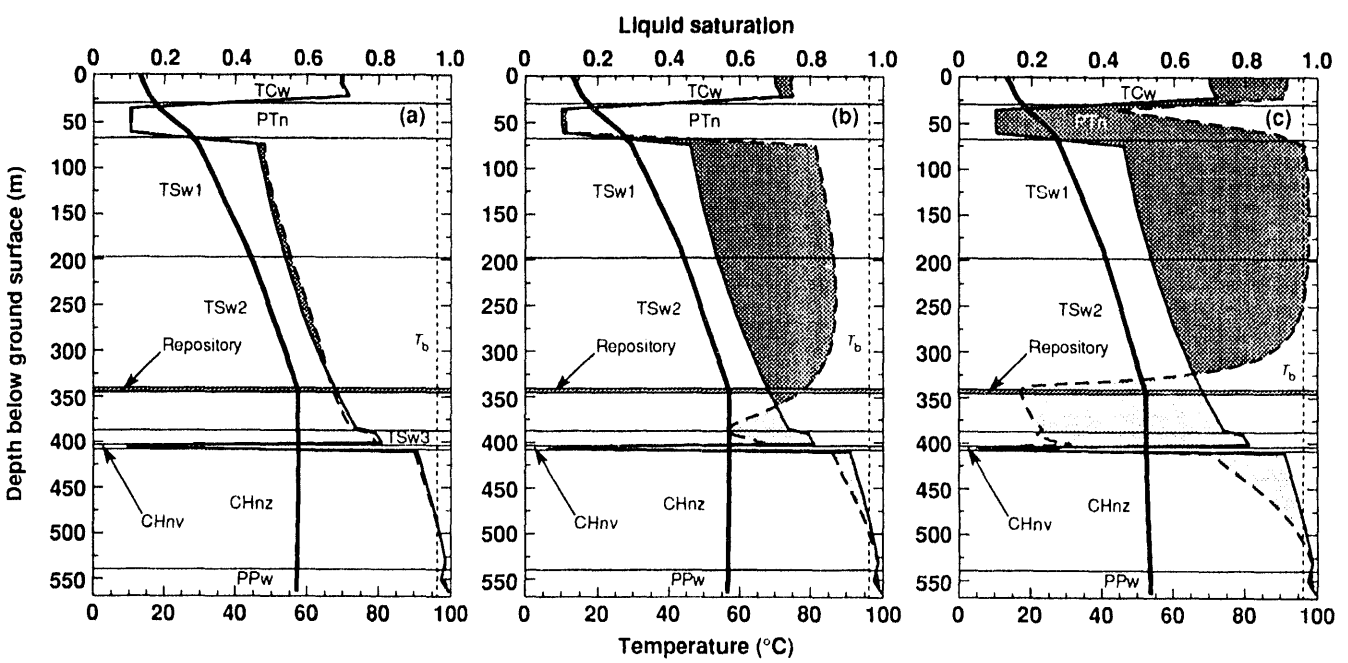

Figure 4. Vertical temperature profile (heavy solid curve) and liquid saturation profile (medium dashed curve) at various radial distances, r, from the repository centerline. Profiles are shown for 10-yr-old SNF, an AML of 49.2 MTU/acre, an APD of 57 kW/acre, and a net recharge flux of 0 mm/yr, including hydrothermal flow in the SZ. (a) $r = 0$ m for $k_b = 280$ millidarcy. (b) $r = 800$ m for $k_b = 10$ darcy. (c) $r = 0$ m for $k_b = 84$ darcy. The medium solid curve represents the initial liquid saturation profile. The light-shaded areas indicate depths that are drier than ambient saturation (dry-out zones), and the dark-shaded areas indicate depths that are wetter than ambient saturation (condensation zones).

the 40-darcy case relative to the 5 darcy. Consequently, thermal performance at the repository center is virtually the same.

Recall that for an AML of 49.2 MTU/acre (the reference SCP-CDR thermal load), increasing k_b from 280 millidarcy to 40 darcy has the effect of decreasing t_{bp} by 74%. The greater sensitivity of thermal performance in the reference SCP-CDR case to this range in k_b is due to two factors. First, because temperatures never significantly exceed boiling, small changes in temperature result in larger changes in t_{bp}. The second factor involves the competition between gas-phase pressure, p_g, differences driven by thermal buoyancy and those driven by boiling. In general, thermal buoyancy occurs because elevated temperatures lighten the column of gas that is within the footprint of the repository. The cooler column of gas outside of the repository footprint is denser and therefore, has a higher p_g at a given depth below the repository horizon. Consequently, cooler, denser gas moves in, displacing the warmer, less dense gas column. In addition to this thermal buoyancy effect, gas-phase pressures in the dry-out zone increase because of boiling. This boiling-generated p_g buildup increases with AML, and it opposes the tendency for thermal buoyancy for some period of time. Therefore, boiling has the effect of suppressing the tendency for thermal buoyancy. For the reference SCP-CDR thermal load, boiling effects are limited in space and time, resulting in less suppression of thermal buoyancy than in the case with a thick, persistent boiling zone.

While mountain-scale, buoyant, gas-phase convection does not significantly affect temperatures at the repository center for an AML of 154.7 MTU/acre, it does reduce temperatures at the edge. At the repository edge, t_{bp} is 4229, 2945, and 1912 yr for the 280-millidarcy, 5-darcy, and 40-darcy cases, respectively. However, mountain-scale, buoyant, gas-phase convection also has a drying effect that is most pronounced at the repository edge. Consequently, the effect of increasing buoyant gas-phase convection is to maintain sub-ambient liquid saturations for a longer period at the edge. Re-wetting back to ambient saturation requires 39,900, 45,000, and 58,300 yr for the 280-millidarcy, 5-darcy, and 40-darcy cases, respectively.

For an AML of 154.7 MTU/acre and $k_b = 1.9$ microdarcy, the maximum gas-phase pressure ($p_g = 22.2$ atm) occurs at the repository center when the temperature peaks ($t_{peak} = 507$ yr). We find in the steam tables[22] that the saturation temperature (equivalent to the boiling temperature) corresponding to $p_g = 22.2$ atm is 217.8°C. Because of the vapor pressure lowering effect due to capillarity, however, the actual boiling temperature is slightly higher. Because of the relatively large k_b in the 280-millidarcy case, p_g does not increase significantly above the ambient p_g (0.896 atm) at the repository, and the actual boiling temperature coincides with $T_b = 96$°C. In general, until heating can drive the liquid saturation to zero, temperatures will be determined by two-phase thermodynamic equilibrium. In the 1.9-microdarcy case, high gas-phase pressures cause the actual boiling temperature to be much greater than T_b, and the thermal load is insufficient to drive water vapor away and thereby lower the saturation to zero; consequently, temperatures continue to be determined by two-phase thermodynamic equilibrium.

For more than a 5 order of magnitude range in k_b (1 millidarcy to 40 darcy), the maximum vertical thickness of the dry-out zone, h_{dz}, only varies 30% for an AML of 154.7 MTU/acre. For this paper, we define the dry-out front as corresponding to the location where the normalized liquid saturation, $\bar{S}_l$, equals 0.9, where $\bar{S}_l$ is defined by

$$\bar{S}_l = \frac{S_l}{S_{l,init}} \qquad (4)$$

where $S_{l,init}$ is the initial liquid saturation. In other words, the dry-out front occurs where S_l is 10% drier than ambient. For the 280-millidarcy case, $h_{dz} = 372$ m; whereas, for the 1-millidarcy case, it is only 23% less ($h_{dz} = 283$ m). Therefore, even for $k_b = 1$ millidarcy, dry-out is not substantially reduced for high AMLs. For the 40-darcy case, $h_{dz} = 403$ m, which is only 8% more than the 280-millidarcy case; whereas, for the 100-microdarcy case it is 46% less ($h_{dz} = 199$ m). Therefore, for more than a 6 order of magnitude range in k_b (100 microdarcy to 40 darcy), h_{dz} only varies by a factor of 2.

When dry-out primarily occurs under boiling conditions (intermediate to high AMLs), we classify thermo-hydrological performance in terms of three major categories and two transitional categories with respect to k_b. The thresholds for these categories depend on AML; however, for the purposes of this discussion we generalize the points at which they occur. We also lump the low-k_b and low-to-intermediate, transitional-k_b categories. A more thorough treatment of the distinctions will be covered in a future paper.

For the low-k_b category ($k_b < 1$ millidarcy), fracture density and connectivity throttle the rate of boiling and dry-out. Because heat flow is dominated by conduction, it is vertically symmetrical about the repository horizon. The low k_b results in large p_g gradients that elevate the boiling temperature, thereby resulting in higher peak temperatures and a temperature profile that is vertically symmetrical about the repository horizon (see $k_b = 1.9$ microdarcy in Fig. 5a).

For the intermediate-k_b category (1 millidarcy $< k_b <$ 1 darcy), the fracture density and connectivity are sufficient to promote boiling that is not throttled by flow resistance in the fractures. Because k_b is not large enough to promote substantial large-scale, buoyant, gas-phase convection, local boiling pressure gradients are dominant, resulting in steam flow and condensate generation that are vertically symmetrical about the repository horizon. Consequently, heat flow continues to be symmetrical about the repository horizon. Convection in the heat-pipe zone has a local, transient effect on the temperature distribution, but because it does not enhance the heat loss from the boiling zone to the sub-boiling zone, t_{bp} is not significantly reduced. Because of two-phase effects, peak repository temperatures are somewhat lower than in the low-k_b category; however, t_{bp} is virtually the same for these two categories.

The intermediate-to-high, transitional-k_b category ($1 < k_b < 5$ darcy) pertains to the range in k_b in which mountain-scale, buoyant, gas-phase gradients begin to dominate local boiling pressure gradients, causing asymmetry in the vertical temperature distribution. For an AML of 154.7 MTU/acre and $k_b = 1$ darcy, we find that steam flow is symmetrical about the repository horizon; whereas, for $k_b = 5$ darcy, steam flow is almost entirely upward. Figure 5a shows the effect that driving all of the steam upward has on the vertical temperature profile. Notice for the 5-darcy case that thermal buoyancy drives the upper boiling front 120 m closer to the ground surface relative to the 1.9-microdarcy case. Also notice the development of a 160-m-thick heat pipe zone. Although convection appears to dominate heat flow in Fig. 4a, we see that the vertical temperature profiles for these two cases are very similar at the end of the boiling period (Fig. 4b). For t_{bp}, the primary concern is the heat balance for the above-boiling zone. Therefore, t_b depends primarily on whether conduction or convection dominates heat flow from the above-boiling to the sub-boiling zone. For the 5-darcy case, buoyant, gas-phase convection in the sub-boiling zone has a negligible affect on heat conservation for the above-boiling zone. Convective processes that occur within the above-boiling zone (e.g., the heat-pipe effect and buoyant, gas-phase flow) affect the above-boiling temperature profile.

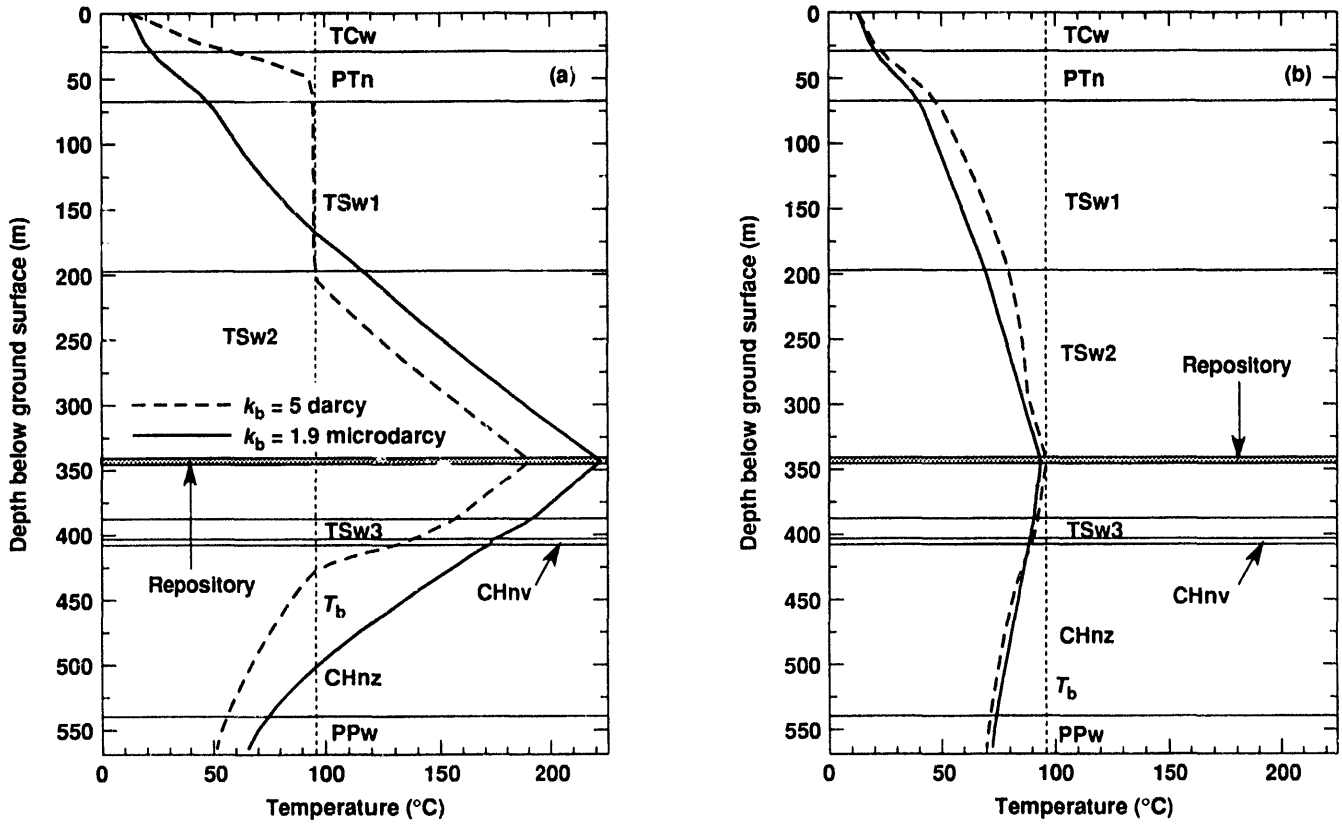

Figure 5. Vertical temperature profile along repository centerline for 30-yr-old SNF, an AML of 154.7 MTU/acre, an APD of 114 kW/acre, and a net recharge flux of 0 mm/yr, including hydrothermal flow in the SZ, at (a) t = 600 yr, and (b) t = 11,500 yr.

For the high-k_b category (k_b>5 darcy), mountain-scale, gas-phase, buoyant convection dominates the direction of steam flow, driving 100% of the steam to the upper condensation zone. However, for the high-AML cases and the range of k_b considered thus far (1.9 microdarcy $\leq k_b \leq$ 40 darcy), the global heat balance for the above-boiling zone is dominated by conduction; therefore, t_b is not substantially reduced relative to the intermediate-k_b or low-k_b categories. For the intermediate-AML cases (e.g., AML=49.2 MTU/acre), because the effects of boiling are limited both in time and space, t_{bp} is substantially reduced by mountain-scale, buoyant, gas-phase convection. For the range of fracture properties considered thus far, the heat-pipe effect was not observed to violate the observation that t_{bp} for the high-AML cases is largely determined by conduction-dominated heat flow. For t_{bp}, the critical concern is whether conduction or convection dominates heat flow from the above-boiling to the sub-boiling zone. It is important to note that because our repository-scale model assumes hydrological properties that are areally homogeneous, these results are indicative of averaged, mountain-scale, thermo-hydrological behavior. In Section III.C, we address the important question of whether heterogeneous fracture connectivity may result in focusing enough condensate in a region of the repository to locally collapse the zone of above-boiling temperatures.

III.B Sub-Repository-Scale, Buoyant, Gas-Phase Flow

Sub-repository-scale, buoyant, gas-phase convection occurs within fracture networks having a connectivity with length-scale comparable to the distance between the hot and cold regions of the repository (Fig. 1a). Buoyant, gas-phase, convection cells develop as the warmer, less dense column of gas within the footprint of the hot WPs is displaced by the cooler, denser column of gas in the adjacent areas (areas without WPs or with cooler WPs). As the initially cooler gas column is heated up, its relative humidity is lowered, causing it to evaporate water from the rock matrix below the hot regions of the repository. This warm moist air is convected upward to where it cools above the repository, generating condensate that drains down fractures back toward the repository and/or is imbibed by the matrix, causing a saturation buildup above the repository. Sub-repository-scale, buoyant, gas-phase convection continues as long as significant temperature differences persist within the repository. We find that it can dominate moisture movement for up to 1000 yr for a center-to-center drift spacing of 38.4 m. These effects will persist longer for larger drift spacing. Given large enough fracture connectivity, mountain-scale, buoyant, gas-phase convection may eventually replace sub-repository-scale convection. Incidentally, at the outer edge of the repository, the distinction between sub-repository-scale and mountain-scale, buoyant, vapor flow is somewhat blurred. Because substantial temperature gradients persist at the outer edge, sub-repository-scale, buoyant, vapor flow may persist for thousands of years even if the fracture connectivity is not sufficient to support substantial mountain-scale convection.

Our sensitivity analysis of sub-repository-scale, buoyant vapor flow included APDs of 10, 20, and 114 kW/acre for 30-yr-old SNF (yielding AMLs of 13.5, 27.1, and 154.7 MTU/acre) and the following values of k_b: 10 millidarcy; and 10, 20, 40, 84, and 168 darcy. We applied the two-dimensional, cross-sectional, drift-scale model described in Section II.F. If WPs are placed end-to-end with a 4.572-m spacing, the thermal load for 27.1 MTU/acre is equivalent to just one pressurized water reactor (PWR) SNF assembly per package.

For 13.5 MTU/acre, the thermal load is equivalent to only one-half of a PWR SNF assembly placed end-to-end down the emplacement drift.

Recall that the threshold bulk permeability, k_b^{hyd}, at which mountain-scale, buoyant, vapor flow begins to dominate moisture movement is about 10 darcy for an AML of 27.1 MTU/acre. Similarly, we found for an AML of 27.1 MTU/acre that k_b^{hyd} is about 10 darcy for sub-repository-scale, buoyant, vapor flow. If k_b > 10 darcy in a fracture network having a connectivity with a length-scale comparable to half the drift spacing (in this example, 19.2 m), then sub-repository-scale, buoyant, vapor flow is sufficient to result in regions of net dry-out below the WPs and net saturation buildup above the WPs. The peak drift-wall temperature, T_{peak}, for this case is 60°C. Although T_{peak} is well below the nominal boiling point, repository-heat-driven flow could result in condensate drainage in the vicinity of WPs for on the order of 1000 yr. For larger drift spacing, temperature differences between the drift-wall and pillar centerline will persist even longer, prolonging the period during which sub-repository-scale, buoyant, vapor flow will drive these effects. For an AML of 13.7 MTU/acre, k_b^{hyd} is about 20 darcy. For this case, although T_{peak} is only 42°C, sub-repository-scale, buoyant, vapor flow may drive significant condensate drainage and saturation buildup effects in the vicinity of WPs. With the ECM, we cannot determine whether the resulting condensate flux results in nonequilibrium fracture flow and water dripping onto WPs. To diagnose the potential for these effects to impact WP performance and radionuclide transport, *in situ* heater tests conducted under sub-boiling conditions will be required.

For an AML of 154.7 MTU/acre, we compared thermo-hydrological behavior for a k_b of 10 and 280 millidarcy; and 84 darcy. For the 84-darcy case, sub-repository-scale, buoyant, vapor flow has a very minor cooling effect, reducing T_{peak} from 196.8 to 195.7°C relative to the 280-millidarcy case. For the 10-millidarcy case, T_{peak} is higher (216.5°C) because of the larger p_g buildup resulting from the smaller k_b. For this range in k_b, the duration of boiling, t_{bp}, is virtually identical (6321, 6340, and 6369 yr for 280 millidarcy, 84 darcy, and 10 millidarcy, respectively). Recall that because the drift-scale model assumes a constant-temperature water table, t_{bp} is less than that predicted by the models that include hydrothermal flow in the SZ. For this range in k_b, we also see no variation in the spatial extent of dry-out. In general, we find that the development of a large above-boiling zone suppresses sub-repository-scale, buoyant, vapor flow. Consequently, sub-repository-scale, buoyant, vapor flow was found to have a negligible impact on thermo-hydrological behavior for an AML of 154.7 MTU/acre.

III.C Focused Vapor and Condensate Flow

Our repository and sub-repository-scale calculations have taken into account a wide range in bulk permeability, k_b. For k_b > 10 millidarcy, we have observed a zone in which the temperature profile is flattened at T_b (≈ 96°C). Higher gas-phase pressures in the boiling zone drive steam away from the repository to where cooler temperatures cause it to condense. Above the repository, much of this condensate is driven back to the boiling zone, primarily by three processes: (1) capillary imbibition in the matrix, (2) capillary imbibition in small-aperture fractures, and (3) gravity drainage in fractures. Gravity drainage in the matrix is insignificant in comparison with matrix imbibition, which is driven by large capillary pressure gradients that arise from saturation gradients in the boiling and condensation zones. Below the repository, only the first two mechanisms (capillary-driven flow in the matrix and fractures) contribute to condensate flow back toward the boiling zone, while the third mechanism (gravity drainage in fractures) tends to drain condensate away from the boiling zone. The return flow of condensate back toward the boiling zone establishes a heat transfer mechanism (driven by the convection of latent heat) called the gravity-driven heat-pipe effect. Given adequately high mass flux rates of the counter-current flow of steam and condensate, heat pipes are capable of sustaining a given heat flux with a much shallower temperature gradient than is associated with heat conduction. Consequently, heat pipes are manifested by a flat temperature profile, with temperatures close to T_b. Pruess and others[23,24] were the first to model the heat-pipe effect in the context of thermo-hydrological performance at Yucca Mountain.

Our repository-scale calculations have generally assumed homogeneous and isotropic k_b. Even for k_b as large as 84 darcy, these calculations have not shown heat pipes resulting in two-phase boiling conditions persisting at the repository horizon under high thermal loads (e.g., AML = 154.7 MTU/acre). Recent analytical work by Nitao and others[25] addresses how focusing condensate into a region of the repository can result in persistent, local, two-phase conditions at the repository horizon. For an AML of 154.7 MTU/acre, they found that if the focusing of condensate drainage and meteoric infiltration results in the local liquid flux being two to three orders of magnitude greater than the mean condensate drainage flux, then two-phase heat-pipe conditions could persist locally at the repository horizon. Because their analysis assumes a smeared heat source, it tends to under-represent the local heat flux in the immediate vicinity of a WP.

To investigate the impact of heterogeneity on the focusing of vapor flow and condensate drainage (and how that focusing affects the development of heat pipes), we used a cross-sectional, drift-scale model and a cross-sectional uniform heat flow (CSUHF) model, which are described in Section II.F. For the drift-scale model, a 1.6-m-wide vertical "fracture zone" is assumed to lie parallel to the WP axis. The k_b of this high-k_b zone is several orders of magnitude larger than k_b throughout the rest of the model (the nominal-k_b zone). The center-to-center spacing between the high-k_b zones is 38.4 m (the same as the center-to-center drift spacing). The CSUHF model represents an infinite series of vertical, uniformly spaced, 1.0-m-wide, high-k_b zones. We considered high-k_b zone spacings of 100 and 1000 m. For the high-k_b zones, we considered 10, 84, 414, and 840 darcy. For the nominal-k_b zones, we considered 1.9 and 100 microdarcy; 1, 10, 100 and 280 millidarcy; and 10 darcy. We report the highlights of this study in this paper. A more detailed discussion will be covered in a future report.

Using the CSUHF model, we considered a suite of cases with an 84-darcy, 1.0-m-wide, fracture zone, 100-m spacing, and nominally fractured rock with the following values of k_b: 100 microdarcy; and 1, 10, 84, and 280 millidarcy. We found that, depending on the contrast in k_b between the high- and nominal-k_b zones, two-phase conditions, resulting in liquid flux, persist in the high-k_b zone at the repository horizon for some period of time. For an AML of 154.7 MTU/acre, local two-phase conditions persist in the high-k_b zone at the repository horizon for 80, 80, 65, 40, and 25 yr for the 100-microdarcy, 1-, 10-, 84-, and 280-millidarcy cases, respectively. The temperature history for the 10-millidarcy case is plotted in Fig. 6c.

The degree of vapor flow focusing into the high-k_b zone, and the resulting duration of two-phase conditions at the repository horizon depend on three factors. First, k_b in the nominally fractured zone must be large enough not to significantly throttle the rate of vapor generation due to boiling (or due to evaporation under sub-boiling conditions). Second, a large contrast in k_b between the high- and nominal-k_b zones results in a gas-phase pressure, p_g, differential between these zones that preferentially drives vapor flow into the high-k_b zone (Fig. 1c). If enough vapor enters and condenses in the high-k_b zone, the return condensate flux will be large enough to maintain two-phase conditions at the repository horizon, possibly resulting in water dripping onto WPs. Third, there must be sufficient spacing between the high-k_b zones to delay, or minimize, the interference between the high-k_b zones with respect to the p_g distribution.

Larger spacing between high-k_b zones allows a greater p_g buildup within the nominal-k_b zone, and increases the duration of this buildup. Moreover, larger spacing allows a greater volume of vapor generation to be focused into the high-k_b zone.

For $k_b = 1$ millidarcy in the nominally fractured rock, vapor generation due to boiling is not throttled; consequently, because it has a larger k_b contrast than the 10-millidarcy case, the net effect is to focus more vapor into the high-k_b zone, resulting in slightly more persistent two-phase conditions at the repository horizon. For the 100-microdarcy case, vapor generation is throttled relative to the 1-millidarcy case; however, because of the larger k_b contrast, there is roughly the same degree of vapor flow focusing, manifested by a similar duration of two-phase conditions at the repository horizon. The larger k_b in the 84-millidarcy case does not produce enough additional vapor flow relative to the 10-millidarcy case to offset the effect of the smaller k_b contrast. Therefore, for 1.0-m-wide, 84-darcy fracture zones, spaced 100 m apart, the greatest degree of vapor and condensate flow focusing occurs if the value of k_b in the nominally fractured rock is somewhere between 100 microdarcy and 1 millidarcy.

The vertical temperature profiles along the centerline of the 1.0-m-wide, 84-darcy zone (x = 0 m) and along the centerline of the 10-millidarcy zone ($x = 50$ m) are plotted in Fig. 7 for an AML of 154.7 MTU/acre. Notice that at $t = 30$ yr, there is no thermal interference between these two locations (Fig. 7a). A heat pipe has developed in the high-k_b zone, manifested by a flat temperature profile, with temperatures close to T_b, that extends vertically nearly 100 m. The temperature profile at $x = 50$ m is the same as that for the case in which k_b is 10 millidarcy everywhere. The similarity with the uniform-k_b case continues until $t = 50$ yr (Fig. 6c), when temperatures at this location abruptly begin to decrease because of the cooling effect of the heat pipes in the high-k_b zones. The heat pipe zones attract heat flow from the rest of the repository horizon. Initially, this preferential heat flow is dominated by gas-phase convection; gradually, it becomes more heavily influenced by heat conduction. The preferential heat flow results in the upper boiling front in the high-k_b zone extending vertically upward well in advance of the mean boiling front. The heat pipe zones effectively function as "cooling fins," the vertical length of the fin being the difference between the depths of the respective boiling fronts at $x = 0$ and 50 m. At $t = 70$ yr, the length of the cooling fin has grown to 88.0 m. The maximum fin length is 98.0 m, occurring at $t = 120$ yr; thereafter, it continually diminishes until $t \approx 700$ yr, when it remains at roughly 20 m.

The effect of the dry-out zone beginning to develop in the high-k_b zone is seen in the temperature profile at $t = 70$ yr (Fig. 7b). Thermal interference between the high- and nominal-k_b zones causes thermal equilibration between these zones (Figs. 7b–f). Within 300 yr, there is essentially no difference in the respective temperature profiles inside the dry-out zone ($T > T_b$).

We also considered a case in which the spacing between the high-k_b zones was increased to 1000 m. This larger spacing has the effect of focusing more vapor flow into the high-k_b zone, thereby, increasing the duration of two-phase conditions in that zone at the repository horizon from 65 to 105 yr. We also considered lower thermal loads for the case with 100-m spacing. For an AML of 77.4 MTU/acre, two-phase conditions persist in the high-k_b zone at the repository horizon for 145 yr (Fig. 6b). For 10-yr-old SNF and an AML of 49.2 MTU/acre, two-phase conditions (with a mobile liquid phase in the fractures) persist for over 600 yr (Fig. 6a), the entire duration of the boiling period at the repository horizon. For other combinations of k_b in the high- and nominal-k_b zones, there was a consistent trend in the duration of two-phase conditions, which increases with decreasing AML.

Of course, this example is highly idealized relative to the complex geometry of real fracture networks, but it illustrates the principle that large contrasts in k_b between neighboring zones can result in focusing of vapor flow and condensate drainage, and, hence, persistent dripping onto WPs. It also illustrates the principle that for a given contrast in k_b, the duration of two-phase conditions increases with spacing between the high-k_b zones. Effectively, the high-k_b

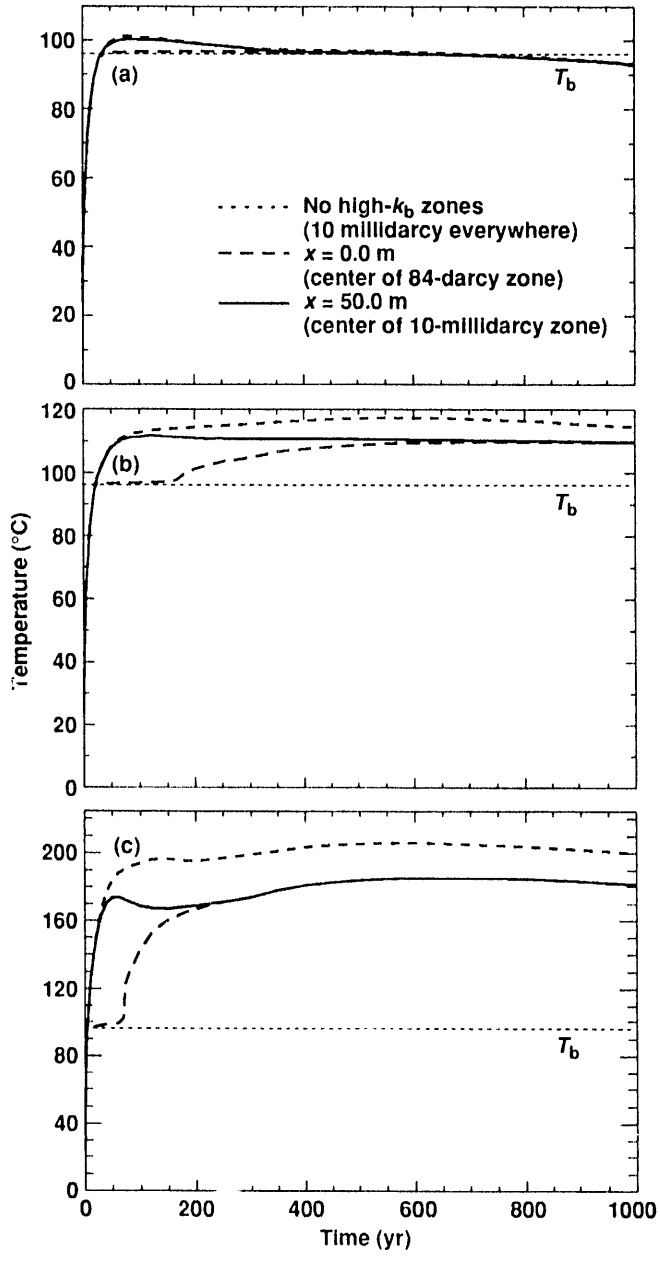

Figure 6. Temperature history at the repository horizon at $x = 0$ m (center of the 1.0-m-wide, 84-darcy zone) and at $x = 50.0$ m (center of the 10-millidarcy zone) for a net recharge flux of 0 mm/yr, including hydrothermal flow in the SZ. The temperature history at the repository center is also plotted for the repository-UZ-SZ-scale model with $k_b = 10$ millidarcy everywhere. (a) 10-yr-old SNF, an AML of 49.2 MTU/acre, and an APD of 57 kW/acre. (b) 30-yr-old SNF, an AML of 77.4 MTU/acre, and an APD of 57 kW/acre. (c) 30-yr-old SNF, an AML of 154.7 MTU/acre, and an APD of 114 kW/acre.

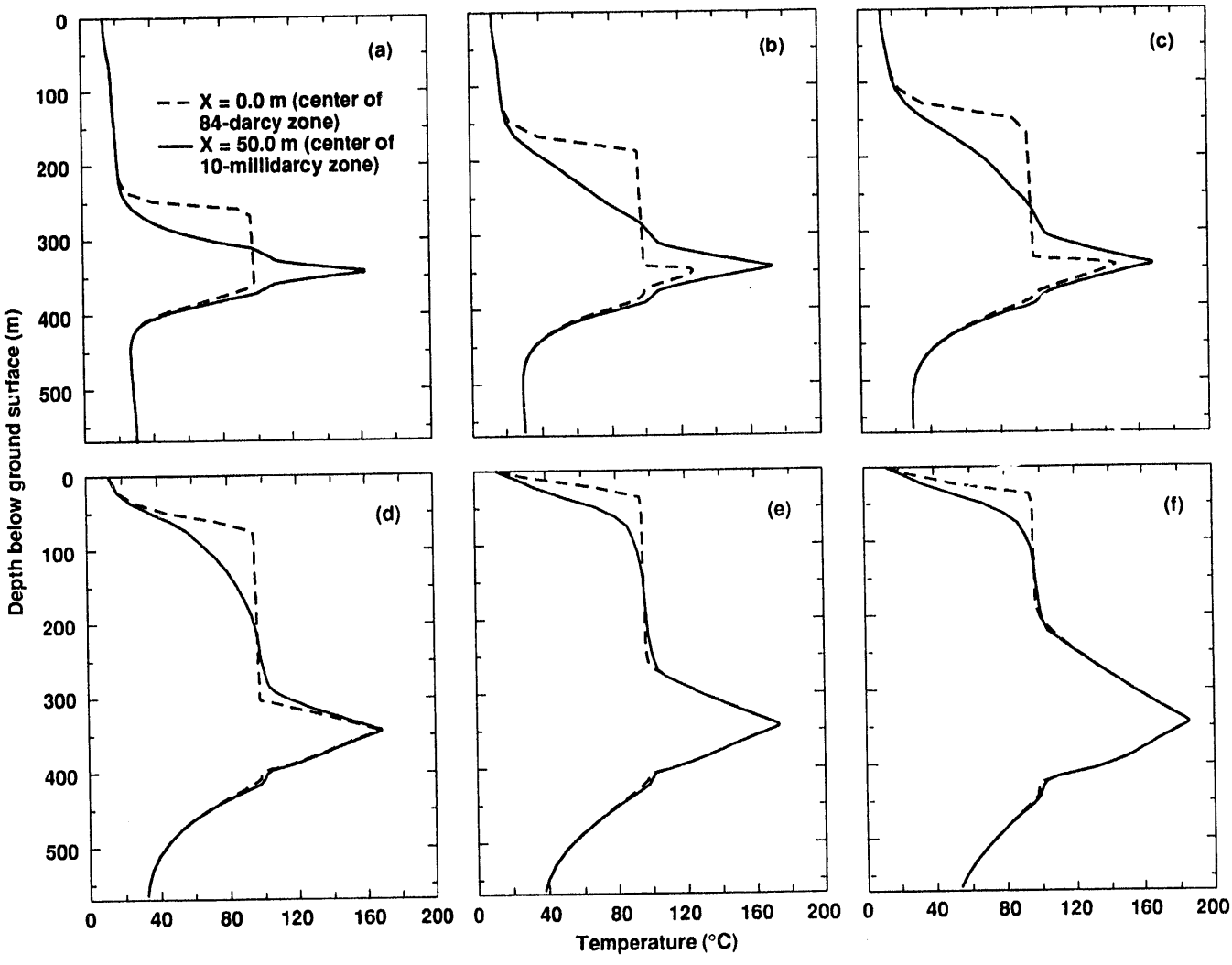

Figure 7. Vertical temperature profile at x = 0 m (center of 1.0-m-wide, 84-darcy zone) and at x = 50.0 m; (center of 10-millidarcy zone) for 30-yr-old SNF, an AML of 154.7 MTU/acre, an APD of 114 kW/acre, a net recharge flux of 0 mm/yr, including hydrothermal flow in the SZ, for (a) t = 30 yr, (b) t = 70 yr, (c) t = 100 yr, (d) t = 200 yr, (e) t = 300 yr, and (f) t = 600 yr.

zones are competing for a finite quantity of vapor flow and condensate generation. Consequently, there is a trade-off between the duration of two-phase conditions and the number of locations where such conditions can occur in the repository. If there are too many such zones, there will be insufficient condensate focusing to cause persistent two-phase conditions at the repository horizon. The degree of focusing necessary to cause persistent two-phase conditions limits the number of locations where such conditions can occur.

We also modeled the case with 84-darcy zones separated by 10-millidarcy zones, using the drift-scale model for AMLs of 49.2, 77.4, and 154.7 MTU/acre. For an AML of 49.2 MTU/acre, we considered both 10- and 20-yr-old SNF. For this model, the high-k_b zones are 1.6 m in width, and the spacing between them is 38.2 m (Fig. 8). We found that, if the k_b contrast is sufficiently large, the p_g differential between these zones drives water vapor back toward the drift and into the high-k_b zone (Fig. 1c). In effect, the emplacement drift functions as a manifold that enhances the gas-phase communication between the high- and nominal-k_b zones. If enough water vapor is focused into the high-k_b zone, then the resulting condensate generation and drainage back down that zone may result in persistent two-phase conditions at the edge of the drift and water dripping onto WPs.

For an AML of 154.7 MTU/acre, two-phase conditions persist at the top of the drift for 8.5 yr (Figs. 8a, 8b, and 9c). For a similar case that was represented with the smeared-heat-flow assumption in the CSUHF model, two-phase conditions persisted for 65 yr in the high-k_b zone at the repository horizon (Fig. 6c). Because the local heat flux in the immediate vicinity of the WP is much greater than the spatially averaged heat flux at the repository, we find that the CSUHF model predicts more persistent two-phase conditions at the repository horizon. We also find that, in spite of persistent two-phase conditions at the top of the drift, the temperature along most of the remainder of the drift wall, the air in the drift, and the WP itself is well above the boiling point. Therefore, although liquid water may be dripping in the drift, the relative humidity of the gas in the drift can still be quite low. At t = 30 yr, the dry-out zones between neighboring drifts have already begun to coalesce (Fig. 8c). Notice that focused vapor flow and condensate drainage causes a very elongated

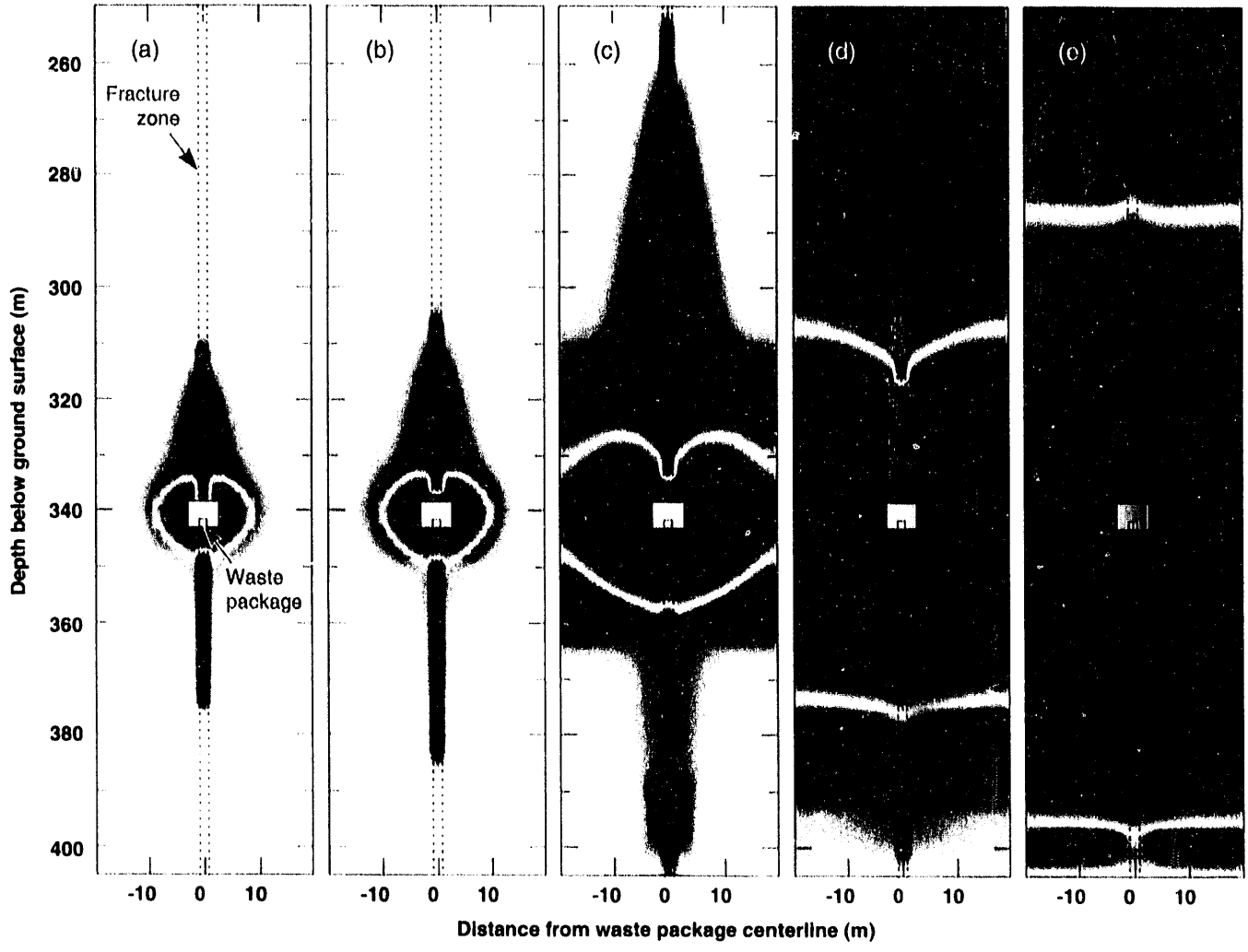

Figure 8. Dimensionless liquid saturation distribution orthogonal to an emplacement drift containing 30-yr-old SNF, for an AML of 154.7 MTU/acre, an APD of 114 kW/acre, and a net recharge flux of 0 mm/yr, assuming a fixed-depth, constant-temperature water table. Distributions are shown at (a) $t = 8$ yr, (b) $t = 10$ yr, (c) $t = 30$ yr, (d) $t = 100$ yr, and (e) $t = 200$ yr. Within the 1.6-m-wide fracture zone, $k_b = 84$ darcy; otherwise, $k_b = 10$ millidarcy. The medium-shaded area surrounding the drift corresponds to a region that is drier than ambient saturation (dry-out zone). The dark-shaded areas correspond to regions that are wetter than ambient saturation (condensation zones). The lighter shading surrounding the dark-shaded area corresponds to a decreasing buildup in saturation (outer edges of condensation zones). No shading indicates no change in saturation.

region of saturation buildup in the vicinity of the high-k_b zone. Also notice that the focused condensate drainage continues to cause a depression in the upper dry-out front. At $t = 100$ yr, the effect of coalescence of the dry-out zones is more pronounced, and focused condensate drainage continues to be manifested by a slight depression in the upper dry-out front (Fig. 8d). Although it is not evident in Figs. 8d and e, the upper condensate front extends well up into the UZ. At $t = 200$ yr, the effect of focused condensate drainage on the upper dry-out front is no longer evident (Fig. 8e), and the dry-out zone is very similar to the 10-millidarcy case with no high-k_b zones.

For an AML of 154.7 MTU/acre, we considered a case that is similar to the previous example, except that k_b in both the high- and nominal-k_b zones is increased by a factor of 10; hence, 1.6-m-wide, 840-darcy zones are separated by 100-millidarcy zones. In spite of the factor of 10 difference in k_b, we find that the thermo-hydrological behavior is nearly the same for these two cases. Therefore, if k_b in the nominal-k_b zone is large enough not to throttle the rate of vapor generation, the primary factor determining the degree of vapor flow and condensate focusing is the k_b contrast between the high- and nominal-k_b zones.

We continue the analysis of cases with 84-darcy zones separated by 10-millidarcy zones. For an AML of 77.4 MTU/acre, two-phase conditions persist at the top of the drift for 38 yr (Fig. 10b), which is considerably less than the 145-yr duration predicted for a similar case by the CSUHF model (Fig. 6b). For 10-yr-old SNF and an AML of 49.2 MTU/acre, two-phase conditions persist at the top of the drift for 60 yr (Figs. 9a, 10a, and 10b); whereas, for a similar case, the CSUHF model predicted more than 600 yr (Fig. 6a), which is the entire duration of the boiling period at the repository horizon. Notice that focused vapor flow and condensate drainage continues to cause a depression in the upper dry-out front (Figs. 10c and d) and preferential drainage in the high-k_b zone below the dry-out zone. It is important to note that an AML of 49.2 MTU/acre is only able to generate marginal boiling conditions; consequently, there is insufficient heat to coalesce the dry-out zones between neighboring drifts. Moreover, the local heat flux from the WP is only, at best,

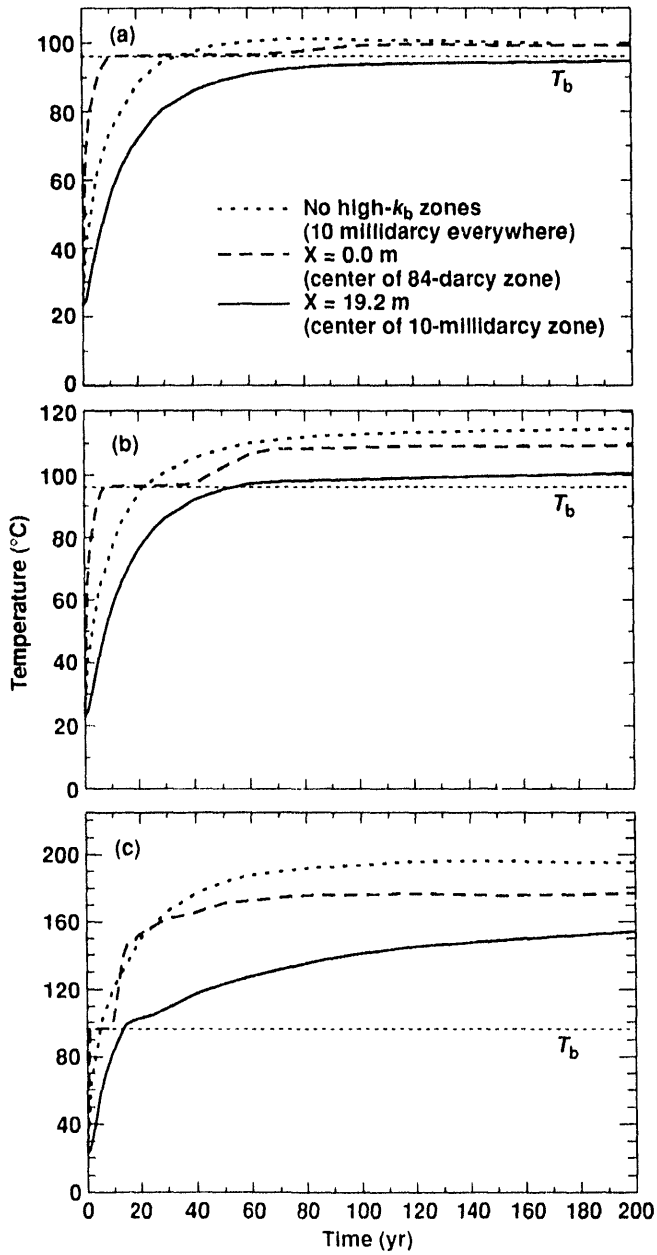

Figure 9. Temperature history on the drift ceiling directly above the waste package (x = 0 m; center of 84-darcy zone) and, for the same depth, at the mid-pillar location (x = 19.2 m; center of 10-millidarcy zone) for a net recharge flux of 0 mm/yr, assuming a fixed-depth, constant temperature water table. The temperature history at the repository center is also plotted for the repository-UZ-SZ-scale model with k_b = 10 millidarcy everywhere. (a) For 10-yr-old SNF, an AML of 49.2 MTU/acre, and an APD of 57 kW/acre (b) For 30-yr-old SNF, an AML of 77.4 MTU/acre, and an APD of 57 kW/acre. (c) For 30-yr-old SNF, an AML of 154.7 MTU/acre, and an APD of 114 kW/acre.

sufficient to drive the re-wetting front in the high-k_b zone 1.5 m away from the top of the drift (Fig. 10c). Following the end of the boiling period, return condensate flow re-wets the top of the drift (Fig. 10e). However, the liquid saturation is less than the critical saturation for a mobile liquid phase in the fractures; consequently, the ECM predicts matrix-dominated condensate drainage at $t \approx 1000$ yr (Fig. 10e). With the ECM, we cannot determine whether this condensate flux results in nonequilibrium fracture flow, and dripping onto WPs.

We also analyzed a 49.2-MTU/acre case, with the subtle difference that it contains 20-yr-old SNF, rather than the 10-yr-old SNF in the previous example. In past studies, we found that long-term, mountain-scale, thermo-hydrological performance primarily depends on AML, and is less sensitive to SNF age. However, at the drift-scale, sub-to-marginal boiling conditions result in thermo-hydrological behavior that is very sensitive to SNF age. For 20-yr-old SNF and an AML of 49.2 MTU/acre, two-phase conditions (with a mobile liquid phase in the fractures) persist at the top of the drift for at least 1575 yr (Fig. 11a–d). At t = 2534 yr, the liquid saturation in the high-k_b zone is quite high relative to ambient conditions (Fig. 11e), although it is less than the critical saturation for a mobile liquid phase in the fractures. However, with the ECM, we cannot determine whether this condensate flux results in nonequilibrium fracture flow, and dripping onto WPs. The effect of gravity-driven refluxing is evident in Figs. 11c–e. Notice that, although focused condensate drainage ceases below the repository horizon, it continues above. The condensate buildup in the high-k_b zone persists for more than 5000 yr. To diagnose the potential for these effects to impact WP performance and radionuclide transport, *in situ* heater tests conducted under sub-boiling and above-boiling conditions will be required.

IV. CONCLUSIONS

With respect to WP performance and radionuclide transport, the only significant source of liquid water is from nonequilibrium fracture flow with three potential origins:

(1) meteoric sources,

(2) condensate generated under *boiling conditions*, and

(3) condensate generated under *sub-boiling conditions*.

The first source of liquid water arises from the ambient system; the second and third sources are generated by repository heat. For a wide range of thermal loading conditions and hydrological properties, we analyze, both at the mountain and sub-repository scales, conditions under which the second and third sources of liquid may be generated.

Mountain-scale, buoyant, gas-phase convection occurs within fracture networks having a connectivity with length-scale comparable to the UZ thickness and repository width. Sub-repository-scale, buoyant, gas-phase convection occurs within fracture networks having a connectivity with length-scale comparable to the distance between the hot and cold regions of the repository. Buoyant, gas-phase, convection cells develop as the warmer, less dense column of gas within the footprint of the heated region is displaced by the cooler, denser column of gas outside of this region. As the initially cooler gas is heated up, its relative humidity is lowered, causing it to evaporate water below the repository. This warm moist air is convected upward

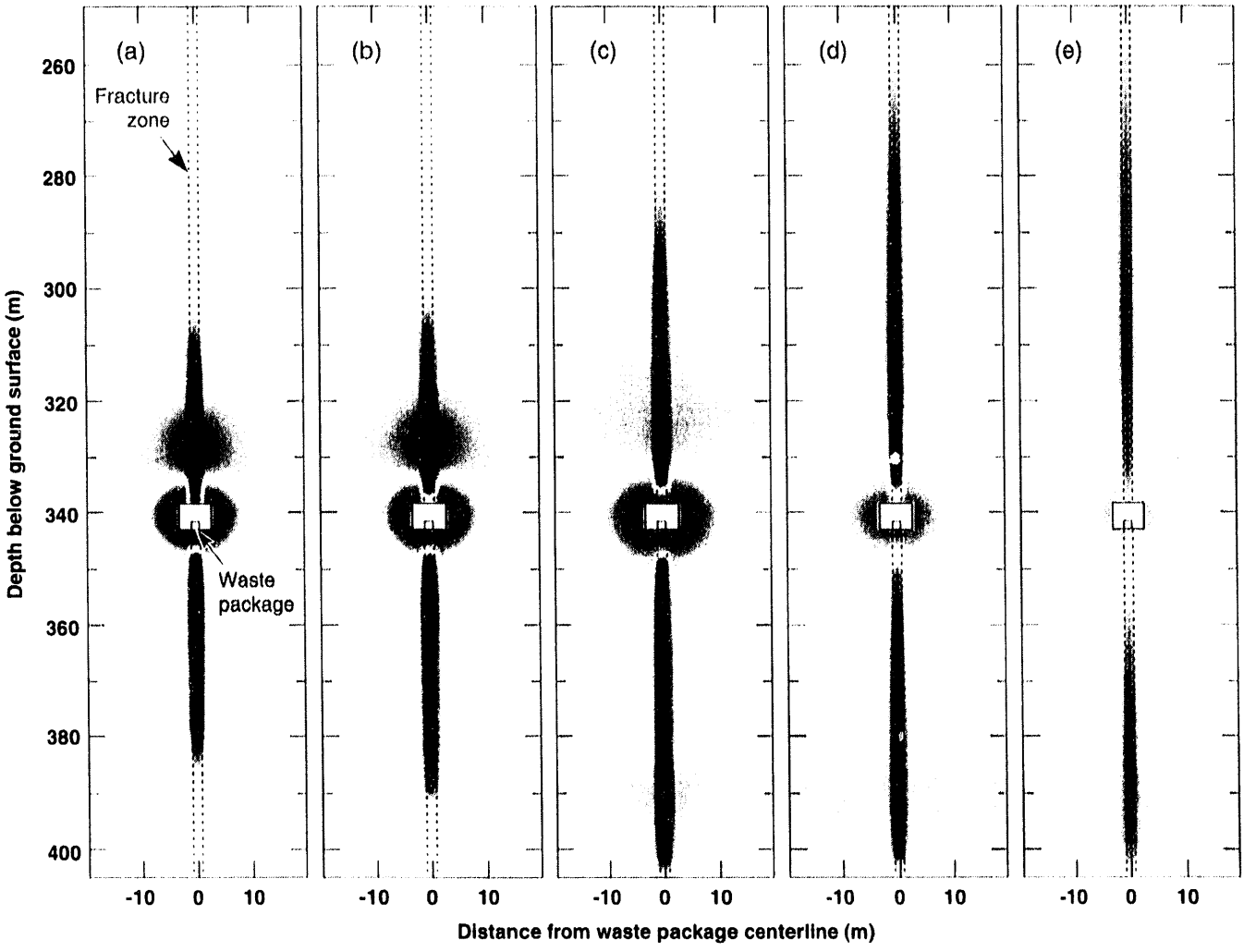

Figure 10. Dimensionless liquid saturation distribution orthogonal to an emplacement drift containing 10-yr-old SNF, for an AML of 49.2 MTU/acre, an APD of 57 kW/acre, and a net recharge flux of 0 mm/yr, assuming a fixed-depth, constant-temperature water table. Distributions are shown at (a) t = 62 yr, (b) t = 71 yr, (c) t = 195 yr, (d) t = 663 yr, and (e) t = 1000 yr. Within the 1.6-m-wide fracture zone, k_b = 84 darcy; otherwise, k_b = 10 millidarcy. The medium-shaded area surrounding the drift corresponds to a region that is drier than ambient saturation (dry-out zone). The dark-shaded areas correspond to regions that are wetter than ambient saturation (condensation zones). The lighter shading surrounding the dark-shaded area corresponds to a decreasing buildup in saturation (outer edges of condensation zones). No shading indicates no change in saturation.

to where it cools above the repository, generating condensate that drains down fractures back toward the repository and/or is imbibed by the matrix, causing a saturation buildup above the repository. Because water removed below the repository may be replenished by water imbibed from the SZ, mountain-scale, buoyant vapor flow can result in a net saturation buildup in the UZ. These effects can dominate moisture movement in the UZ on the order of 100,000 yr. Sub-repository-scale, buoyant, gas-phase convection continues as long as significant temperature differences persist within the repository. We find that it can dominate moisture movement for up to 1000 yr for a center-to-center drift spacing of 38.4 m. These effects will persist longer for larger drift spacing.

By considering a wide range in bulk permeability, k_b, we identify the threshold k_b (called k_b^{hyd}) at which buoyant, vapor convection begins to dominate hydrological behavior, and the threshold k_b (called k_b^{th}) at which this convection begins to dominate thermal behavior. We find that k_b^{hyd} is roughly the same for mountain-scale and sub-repository-scale, buoyant, gas-phase flow. We also find that k_b^{th} is generally an order of magnitude larger than k_b^{hyd}. The development of a large above-boiling zone is shown to suppress the effects of buoyant, vapor flow, both on the mountain and sub-repository scales.

Zones of sharply contrasting k_b are also found to influence condensate generation and drainage. We find that if the contrast in k_b between the high-k_b zone and the rest of the rock surrounding the emplacement drift (called the nominal-k_b zone) is sufficiently large, then the p_g differential between these zones drives water vapor back toward the drift and into the high-k_b zone. In effect, the emplacement drift functions as a manifold that enhances the gas-phase communication between the high-k_b and nominal-k_b zones. If enough water vapor is driven into the high-k_b zone, then the resulting condensate generation and drainage back down that zone may result in persistent two-phase conditions at the edge of the drift and water dripping onto WPs. These effects can occur under both sub-boiling and boiling conditions. Large-scale *in situ* heater tests, conducted under both sub-boiling and boiling conditions, are needed to determine the potential for these effects to impact WP performance and radionuclide transport.

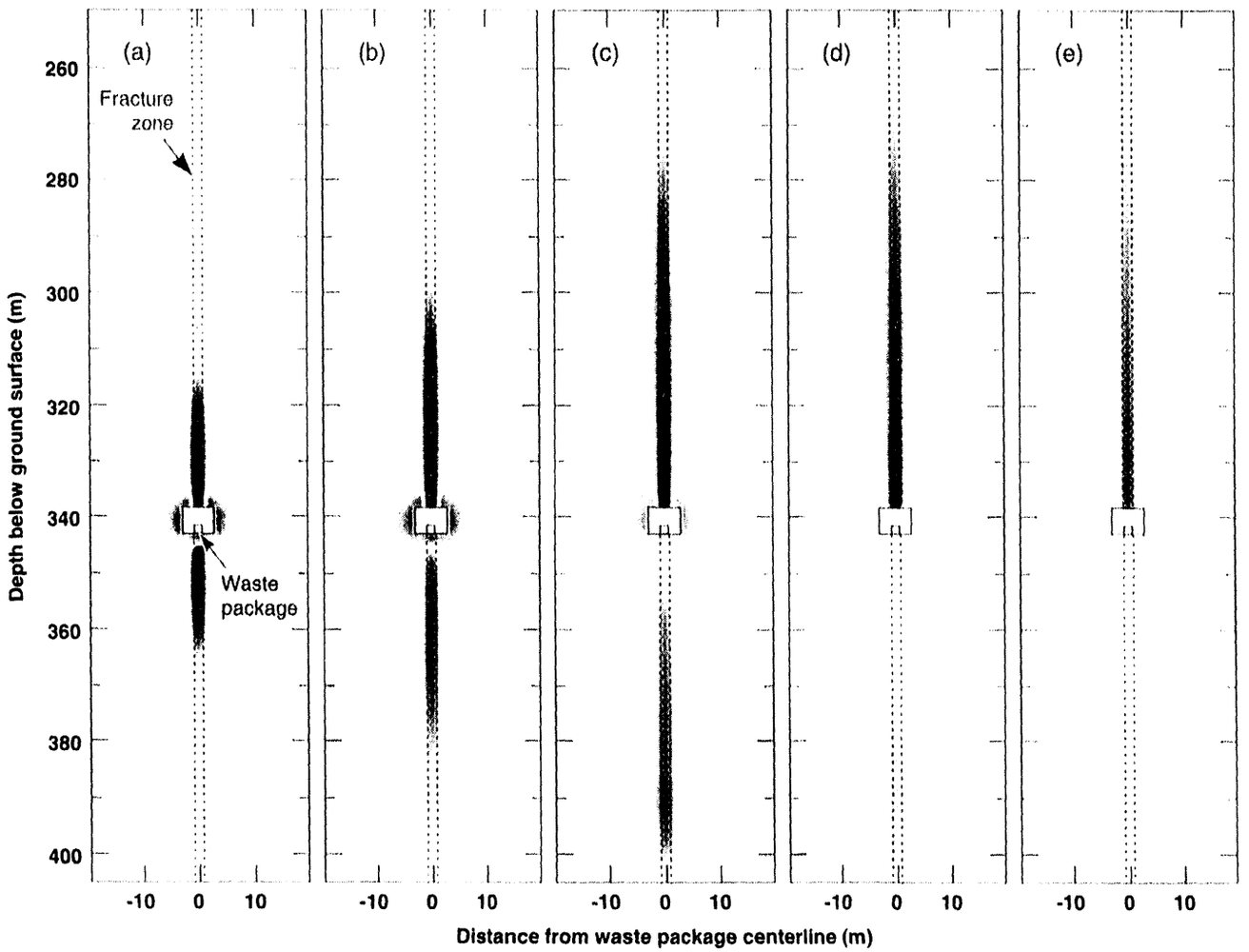

Figure 11. Dimensionless liquid saturation distribution orthogonal to an emplacement drift containing 20-yr-old SNF, for an AML of 49.2 MTU/acre, an APD of 43.7 kW/acre, and a net recharge flux of 0 mm/yr, assuming a fixed-depth, constant-temperature water table. Distributions are shown at (a) t = 59 yr, (b) t = 159 yr, (c) t = 661 yr, (d) t = 1575 yr, and (e) t = 2534 yr. Within the 1.6-m-wide fracture zone, k_b = 84 darcy; otherwise, k_b = 10 millidarcy. The medium-shaded area surrounding the drift corresponds to a region that is drier than ambient saturation (dry-out zone). The dark-shaded areas correspond to regions that are wetter than ambient saturation (condensation zones). The lighter shading surrounding the dark-shaded area corresponds to a decreasing buildup in saturation (outer edges of condensation zones). No shading indicates no change in saturation.

It should be noted that we may have considered very extreme examples of heterogeneity. However, the same degree of heterogeneity was considered for a wide range of thermal loads, yielding very different outcomes. The two-phase effects of focused vapor flow and condensate drainage are seen to be more persistent in the vicinity of WPs for marginal boiling cases, and continue long after temperatures have dropped below the boiling point. For increasing AML, the effects of focused vapor flow and condensate drainage were decreasingly persistent. For high AMLs, the effects of focused vapor and condensate drainage virtually vanished, long before temperatures dropped below the boiling point. In this paper, we have begun to address condensate focusing that arises from preferential, gas-phase focusing. In future reports, we will address condensate focusing that arises from preferential, liquid-phase focusing of condensate, as well as from combinations of gas-phase and liquid-phase focusing, including consideration of infiltration from meteoric sources. The potential impact that meteoric infiltration may have on liquid-phase flow focusing will increase with time as the decaying heat load from the repository causes the mean condensate flux to decrease. Clearly, the challenge of adequately understanding repository-heat-driven, vapor and condensate flow is at least as formidable for sub-boiling conditions as it is for above-boiling conditions.

ACKNOWLEDGMENTS

The authors acknowledge the helpful suggestions of Jim Blink during the past year and the review of Richard Knapp. We also appreciate the assistance of Rick Wooten, who prepared the graphics, and the editorial assistance of Jay Cherniak, Elaine Price, and Sue Stull. This work was supported by the Near-field Hydrology Task (WBS 1.2.2.2.2) of the Yucca Mountain Site Characterization Project. Work performed under the auspices of the U.S. Department of Energy by Lawrence Livermore National Laboratory under Contract W-7405-Eng-48.

REFERENCES

1. Buscheck, T.A., and J.J. Nitao, "The Impact of Thermal Loading on Repository Performance at Yucca Mountain," American Nuclear Society, *Proceedings Third International High-Level Radioactive Waste Management Conference*, Las Vegas, NV, April 12-16, 1992. Also, *UCRL-JC-109232*, Lawrence Livermore National Laboratory, Livermore, CA, (1992).

2. Buscheck, T.A., and J.J. Nitao, "The Impact of Repository-Heat-Driven Hydrothermal Flow on Hydrological Performance at Yucca Mountain," American Nuclear Society, *Proceedings Fourth International High-Level Radioactive Waste Management Conference*, Las Vegas, NV, April 1993. Also, *UCRL-JC-112444*, Lawrence Livermore National Laboratory, Livermore, CA (1993).

3. Buscheck, T.A., and J.J. Nitao, "Repository-Heat-Driven Hydrothermal Flow at Yucca Mountain, Part I: Modeling and Analysis," *Nuclear Technology*, Vol. 104, No. 3, pp. 418-448, (1993).

4. Montazer, P., and W.E. Wilson, "Conceptual Hydrologic Model of Flow in the Unsaturated Zone, Yucca Mountain, Nevada," Water Resources Investigation Report 84-4345, U.S. Geological Survey (1984).

5. Klavetter, E.A., and R.R. Peters, "Estimation of Hydrologic Properties of an Unsaturated Fracture Rock Mass," *SAND84-2642*, Sandia National Laboratories, Albuquerque, NM (1986).

6. Buscheck, T.A., J.J. Nitao, and D.A. Chesnut, "The Impact of Episodic Nonequilibrium Fracture-Matrix Flow on Geological Repository Performance," *Proceedings American Nuclear Society Topical Meeting on Nuclear Waste Packaging (Focus 91)*, Las Vegas, NV, Sept. 30-Oct. 2, 1991. Also, *UCRL-JC-106759*, Lawrence Livermore National Laboratory, Livermore, CA, 1991.

7. DOE (U.S. Dept. of Energy), "Yucca Mountain Project Reference Information Base," *YMP/CC-0002 (Version 04.002)*, Nevada Operations Office, Las Vegas, NV (1990).

8. Nitao, J.J., "Theory of Matrix and Fracture Flow Regimes in Unsaturated, Fractured Porous Media," American Nuclear Society, *Proceedings Second High-Level Radioactive Waste Management Conference*, Las Vegas, NV, April 28-May 2 1991. Also, *UCRL-JC-104933*, Lawrence Livermore National Laboratory, Livermore, CA (1991).

9. Norris, A.E., "The Use of Chlorine Isotope Measurements to Trace Water Movements at Yucca Mountain," *Proceedings American Nuclear Society Topical Meeting on Nuclear Waste Isolation in the Unsaturated Zone (Focus 89)*, Las Vegas, NV, Sept. 17-21, 1989.

10. Ramirez, A.L., T.A. Buscheck, R. Carlson, W. Daily, K. Lee, W. Lin, N. Mao, T.S. Ueng, H. Wang, and D. Watwood, "Prototype Engineered Barrier System Field Test (PEBSFT) Final Report," *UCRL-ID-106159*, Lawrence Livermore National Laboratory, Livermore, CA (1991).

11. Buscheck, T.A., and J.J. Nitao, "Estimates of the Width of the Wetting Zone Along a Fracture Subjected to an Episodic Infiltration Event in Variably Saturated, Densely Welded Tuff," *UCID-21579*, Lawrence Livermore National Laboratory, Livermore, CA (1988).

12. Buscheck, T.A., and J.J. Nitao, "Modeling Hydrothermal Flow in Variably Saturated, Fractured, Welded Tuff During the Prototype Engineered Barrier System Field Test of the Yucca Mountain Project," *Proceedings of the Fifth NRC Workshop on Flow and Transport through Unsaturated Fractured Rock*, University of Arizona, Tuscon, AZ, Jan 7-10, 1991, Also, *UCRL-ID-106521*, Lawrence Livermore National Laboratory, Livermore, CA (1991).

13. Nitao, J.J., "V-TOUGH - An Enhanced Version of the TOUGH Code for the Thermal and Hydrologic Simulation of Large-Scale Problems in Nuclear Waste Isolation," *UCID-21954*, Lawrence Livermore National Laboratory, Livermore, CA (1989).

14. Pruess, K., "TOUGH User's Guide," *NUREG/CR-4645*, Nuclear Regulatory Commission (1987).

15. Peters, R.R., E.A. Klavetter, I.J. Hall, S.C. Blair, P.R. Hellers, and G.W. Gee, "Fracture and Matrix Hydrologic Characteristics of Tuffaceous Materials from Yucca Mountain, Nye County, Nevada," *SAND84-1471*, Sandia National Laboratories, Albuquerque, NM (1984).

16. SNL (Sandia National Laboratories), "Site Characterization Plan - Conceptual Design Report," *SAND84-2641*, Sandia National Laboratories, Albuquerque, NM (1987).

17. Pruess, K., and Y.W. Tsang, "Modeling of Strongly Heat-Driven Processes at a Potential High-Level Nuclear Waste Repository at Yucca Mountain, Nevada," *Proceedings Fourth International High-Level Radioactive Waste Management Conference*, Las Vegas, NV, April 1993.

18. Konikow, L.F., and J.D. Bredehoeft, "Ground-water Models Cannot Be Validated," *Advances in Water Resources*, Vol. 15, pp. 75-83 (1992).

19. Buscheck, T.A., D.G. Wilder, and J.J. Nitao, "Large-Scale In Situ Heater Tests for the Characterization of Hydrothermal Flow at Yucca Mountain," American Nuclear Society, *Proceedings Fourth International High-Level Radioactive Waste Management Conference*, Las Vegas, NV, April 1993. Also, *UCRL-JC-112445*, Lawrence Livermore National Laboratory, Livermore, CA, (1993).

20. Buscheck, T.A., D.G. Wilder, and J.J. Nitao, "Repository-Heat-Driven Hydrothermal Flow at Yucca Mountain, Part II: Large-Scale In Situ Heater Tests," *Nuclear Technology*, Vol. 104, No. 3, pp. 449-471 (1993).

21. Weeks, E.P., personal communication, U.S.G.S. (1993).

22. Keenan, J.H., F.G. Keyes, P.G. Hill, and J.G. Moore, *Steam Tables: Thermodynamic Properties of Water Including Vapor, Liquid, and Solid Phases*, John Wiley and Sons, Inc, New York, NY (1969).

23. Pruess, K., Y.W. Tsang, and J.S.Y. Wang, "Numerical Studies of Fluid and Heat Flow Near High-Level Nuclear Waste Packages Emplaced in Partially Saturated Fractured Tuff," *LBL-18552*, Lawrence Berkeley Laboratory, Berkeley, CA (1984).

24. Pruess, K., J.S.Y. Tsang, and Y.W. Tsang, "On Thermohydrologic Conditions Near High-Level Nuclear Wastes Emplaced in Partially Saturated Fractured Tuff, Part 1: Simulation Studies With Explicit Consideration of Fracture Effects," *Water Resources Research*, Vol. 26, No. 6, pp. 1235-1248 (1990).

25. Nitao, J.J, R.M. Bradford, and W.J. O'Connell, "Modeling the Heterogeneity of Condensate Flux through a Heated Repository," *UCRL-ID-115412*, Lawrence Livermore National Laboratory, Livermore, CA (1993).

DATE
FILMED
2/10/94
END